Origin of Reactivity Trends of an Elusive Metathesis Intermediate from NMR Chemical Shift Analysis of Surrogate Analogs

Yuya Kakiuchi, Scott R. Docherty, Zachariah J. Berkson, Alexander V. Yakimov, Michael Wörle, Christophe Copéret,* Sadig Aghazada*

ETH Zurich, Department of Chemistry and Applied Biosciences, CH-8093. Zurich, Switzerland.

ABSTRACT: Olefin metathesis has been established as an efficient tool to build carbon-carbon bonds, and its widespread applications in organic synthesis have been made possible by the development of efficient homogeneous catalysts – Grubbs and Schrock-type – that operate through the same intermediates and Chauvin mechanism. With d^0 Schrock-type catalysts, the first elementary step, olefin-coordination, is often rate determining, but it been rarely explored due to the lack of accessible relevant molecular analogs. Here, we develop a surrogate of this key olefin-coordination intermediate, namely a cationic d^0 tungsten oxo-methylidene complex bearing two *N*-heterocyclic carbene ligands, $[WO(CH_2)Cl(IMes)_2](OTf)$ (**1**) (IMes = 1,3-dimesitylimidazole-2-ylidene; OTf – triflate counter-anion) resulting in a trigonal bipyramidal (TBP) geometry, along with its neutral octahedral analog $[WO(CH_2)Cl_2(IMes)_2]$ (**2**), and an isostructural oxo-methylidyne derivative $[WO(CH)Cl(IMes)_2]$ (**3**). These compounds were fully characterized by state-of-the-art methods, including single-crystal X-ray diffraction (scXRD) and multinuclear (^1H, ^{13}C, ^{183}W) solution NMR spectroscopy. The analysis of their solid-state ^{13}C and ^{183}W MAS NMR signatures, along with computed ^{17}O NMR parameters, helps to correlate their electronic structures with NMR patterns and evidences the importance of the competition between the three equatorial ligands in the TBP complexes. Further analysis validates the suitability of complex **1** as a surrogate molecule to interrogate the electronic structure of the key olefin coordination intermediate of the Chauvin cycle. Anchored on experimentally obtained NMR parameters for **1**, computational analysis of a series of olefin coordination intermediates highlights the interplay between σ- and π-donating ligands in modulating the stability of TBP olefin-coordination intermediates, paralleling their reactivity. In this work, NMR spectroscopy descriptors reveal the origin for the advantage of the dissymmetry in σ-donating abilities of ancillary ligands in Schrock-type catalysts: weak σ-donors avoid the orbital-competition with the oxo ligand upon formation of a TBP olefin-coordination intermediate, while stronger σ-donors compromise M≡O triple bonding and thus render olefin coordination step energy expensive.

INTRODUCTION

Olefin metathesis has become a key technology of the chemical industry, spanning a broad range of applications.[1-5] While metathesis has been used for petrochemicals since its original discovery in the 1960s,[6-11] it has only been relatively recently implemented in industry for fine chemicals.[12] This implementation has paralleled the development of efficient molecular catalysts based on both early and late transition metal alkylidenes, the so-called Schrock (Mo, W, Re) and Grubbs-type (Ru) catalysts.[13-16] These catalysts operate through the Chauvin mechanism, which involves a [2+2]-cycloaddition between the olefin and an alkylidene (and its associated reverse step), generating a metallacyclobutane with a trigonal bipyramidal (TBP) geometry as a key intermediate (Figure 1a).[17-22] Notably, despite the apparent difference in electronic configuration between d^0 Schrock- and d^4 Grubbs-type metathesis catalysts, both form TBP metallacyclobutane intermediates with similar and unusual ^{13}C NMR signatures. Combined with theoretical calculations, these unexpectedly common NMR signatures were connected to similar and specific electronic structures for these intermediates (Figure 1b), hence highlighting the power of NMR chemical shifts as descriptors of reactivity. Recently, such analyses of NMR chemical shifts were applied, beyond conventional ligand-centered approaches, i.e. to metal-centered NMR techniques.[23-38]

Another key step in metathesis, more rarely discussed (and often not written out in reaction mechanisms), is the coordination of the olefin to the metal site. For Schrock-type catalysts [M(E)(=CHR)(X)(Y)], with M = Mo or W, X and Y = monoanionic ligands, and E = imido or oxo (X can be substituted by an *N*-heterocyclic carbene (NHC) in cationic complexes), olefin coordination requires significant structural reorganization considering that the starting catalysts are tetrahedral d^0 complexes with no empty coordination site. Computational studies have highlighted that a key requirement for coordination and subsequent [2+2]-cycloaddition is to place the stronger σ-donating X or NHC ligand *trans* to the incoming olefin while having the alkylidene, Y and E ligands on the equatorial plane of this overall TBP intermediate.[18-19] Earlier studies pointed out that this olefin-coordination step, with concomitant structural re-organization from tetrahedral to TBP geometry, is a highly energy-demanding process that is often a rate-determining step.[18-19] While the origin of such a high barrier can be computationally traced back to placing three ligands (E, Y, and the alkylidene) in the basal plane of the TBP geometry, there is currently hardly any experimental data regarding this intermediate. This is due to the lack of available molecular analogs: while detected by solution NMR as transient species, isolation of an olefin complex for a d^0 transition metal, and Schrock

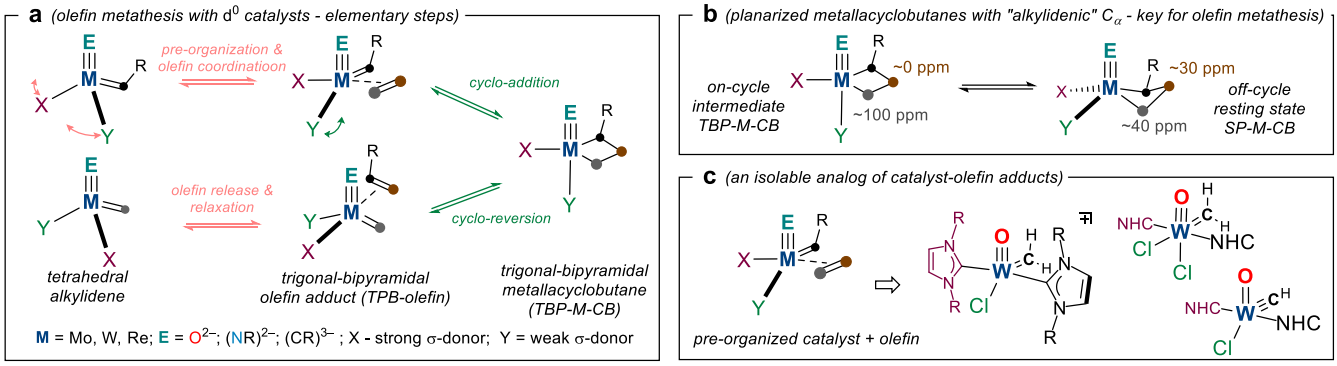

Figure 1. (**a**) proposed structural transformations upon olefin coordination and cycloaddition; (**b**) ^{13}C NMR signatures of metathesis active and off-cycle metallacyclobutane intermediates; (**c**) surrogate structures to address the olefin coordination elementary step.

alkylidenes in particular, has been challenging.[39-42] Thus, to analyze the first elementary step of the olefin metathesis cycle, i.e. olefin coordination, we herein developed a suitable and stable surrogate compound, and established its electronic structure using ligand- and metal-centered NMR approaches.

Employing an NHC as a σ-donor and π-acceptor ligand, formally being isolobal to an olefin at a d^0 metal, we have been able to construct the desired surrogate complex derived from cationic Schrock alkylidenes, specifically of the class of Buchmeiser olefin metathesis catalysts, having a second NHC stabilizing ligand in *trans* position.[42-51] This cationic trigonal bipyramidal tungsten oxo-methylidene complex (**1**), along with neutral octahedral oxo-methylidene (**2**) and isostructural oxo-methylidyne (**3**) analogs provide basis to assess the details of the first step of olefin metathesis catalysis, based on the analysis of ^{13}C and ^{183}W solid-state NMR spectra, augmented by computations. This study provides detailed picture for the olefin (de-)coordination step addressing its electronic structure and the role of ligand sets that are compensating the coordination sphere: alkylidene, E-type ligand, and a pair of strong and weak σ-donor ligands

RESULTS

Synthesis and characterization.

Herein, we developed a novel route toward the desired cationic oxo-methylidene complex **1**, namely $[WO(CH_2)Cl(IMes)_2](OTf)$, along with neutral oxo-methylidene **2** – $[WO(CH_2)Cl_2(IMes)_2]$, and oxo-methylidyne complex **3** – $[WO(CH)Cl(IMes)_2]$, (IMes = 1,3-dimesitylimidazole-2-ylidene; OTf – triflate counter-anion). This series of complexes was accessed starting from a novel d^2 W(IV)-oxo complex **4** stabilized with two NHC ligands, namely $[WOCl_2(IMes)_2]$, as illustrated in Scheme 1. The diamagnetic complex **4** forms in moderate yields either upon reduction of $WOCl_4$ with KC_8 in the presence of two equivalents of free carbene, or upon substitution of phosphine ligands in $[WOCl_2(PPh_2Me)_3]$ with two equivalents of free carbene.[52-53] Complex **4** is among the rare low-valent tungsten NHC complexes[54] and is the only NHC-stabilized W(IV)-oxo complex reported to date. The reaction of **4** with two equivalents of methylenetriphenylphosphorane (Ph_3PCH_2) results in a magenta-colored oxo-methylidyne complex **3**, namely $[WO(CH)Cl(IMes)_2]$, in moderate yields. Notably, though complexes with a terminal methylidyne ligand are known for mid-transition metals,[55-71] complex **3** features an unusual combination of the two simplest (potential) six-electron donor oxo and methylidyne ligands bound to a single metal. Protonation of **3** with lutidinium chloride results in a slightly yellow compound **2** – $[WO(CH_2)Cl_2(IMes)_2]$ in high yields, while reaction with lutidinium triflate yields the target oxo-methylidene compound **1** – $[WO(CH_2)Cl(IMes)_2](OTf)$ quantitatively as a colorless crystalline product.

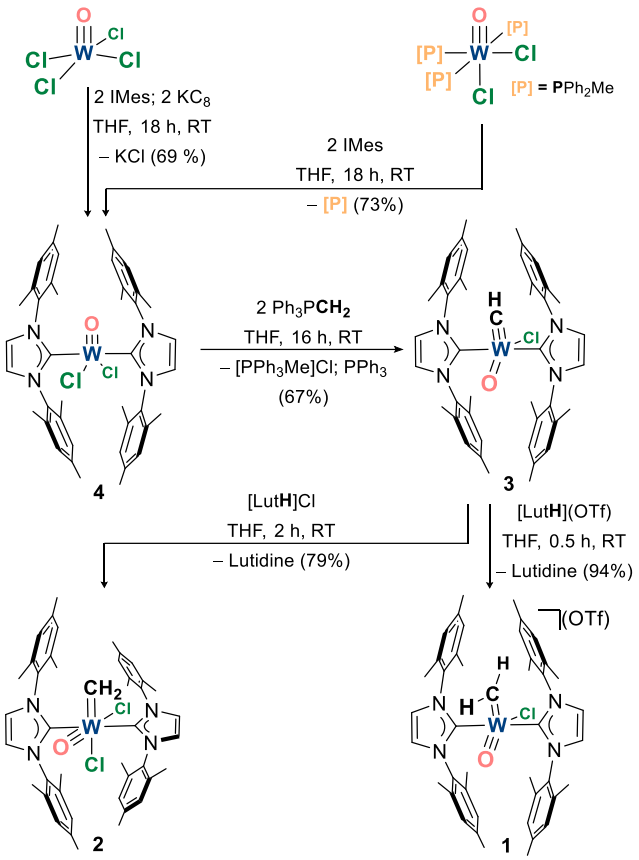

Scheme 1. Synthesis of W(IV)-oxo precursor **4**, and its conversion to W(VI) oxo-methylidyne **3** and oxo-methylidene complexes **2** and **1**.

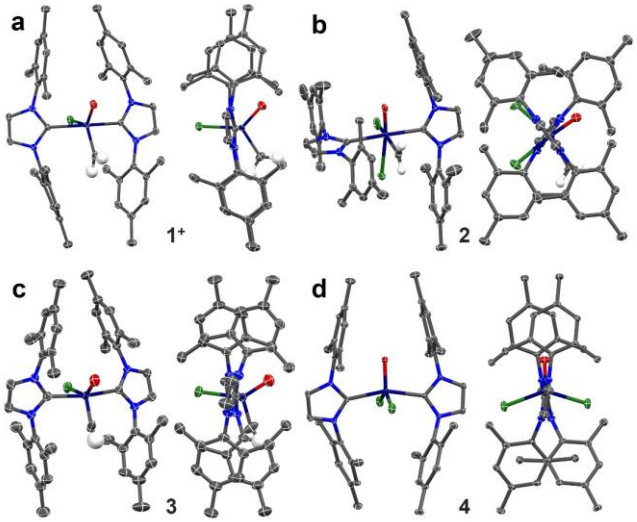

Figure 2. (**a**) The molecular structures of complex cation **1**+ in crystals of $[WO(CH_2)Cl(IMes)_2](OTf)\times(THF)$, (b) **2** in crystals of $[WO(CH_2)Cl_2(IMes)_2]\times(benzene)$; (**c**) one of the better resolved molecules of **3** in crystals of $2\times[WO(CH)Cl(IMes)_2]\times(pentane)$; and (**d**) **4** in crystals of $[WOCl_2(IMes)_2]$. All structures are illustrated in two perspective views. Solvent molecules, counterions, and all hydrogen atoms except those at methylidene or methylidyne ligands are omitted for clarity. The color code: W – navy, O – red, Cl – green, N – blue, C – grey, H – light grey.

Single crystals of all four new compounds were analyzed with X-ray diffractometry (Figure 2). Analysis of colorless crystals of compound **1** reveals a cationic trigonal bipyramidal complex with non-ligated triflate counterion. Oxo, chloride, and the methylidene ligand, with its two hydrogen atoms located in the Fourier difference map and freely refined, form the equatorial plane around central tungsten of the TBP complex. In contrast, complex **2** features a *pseudo*-octahedral geometry with *cis*-positioned oxo and methylidene ligands and two axial and nearly orthogonal NHC ligands. Magenta-colored crystals of **3** revealed two crystallographically independent oxo-methylidyne complexes in an asymmetric unit. The tungsten center in the first molecule is disordered over two positions with occupancies of 97.3 and 2.7 %, while in the second molecule a more complex disorder is observed (for detailed analysis and discussion on the origin of the disorder see the SI file, chapter 2). A dichroic green-purple crystal of **4** revealed a trigonal bipyramidal complex with two axial NHC ligands and a crystallographically imposed rotation axis along the W–O connection. Overall, for all four complexes presented herein, spatial orientations of the NHC ligands are defined by the interactions between their π-systems and chloride ligands.[72] The close inspection of W–O and W–$C_{CH/CH2}$ bond lengths across the series of oxo-methylidene/dyne complexes reveals complementary trends. The oxo-methylidene complexes show long W–C_{CH2} bond lengths (1.915(3) Å in **1**; 2.007(6) Å and 1.997(7) Å for two disordered orientations in **2**) and short W–O distances (1.689(2) Å in **1**; 1.683(4) Å and 1.638(5) Å for two disordered orientations in **2**). The oxo-methylidyne complex **3** reveals W–C_{CH} and W–O distances which fall within the range between W–C_{CH2} and W–O distances of oxo-methylidene complexes. These structural parameters along with the analysis of computational Mayer bond orders highlight the capacity of the oxo-ligand to partially rehybridize from *sp* to *sp²* and facilitate the bonding of tungsten with other ligands (SI file, chapter 2).[73-75]

All the species were also characterized with multi-nuclear solution NMR techniques (Figure S23). Remarkably, the coordinating carbon atom of NHC ligands are more shielded in W(VI) species (195, 192, and 197 ppm in **1**, **2**, and **3** respectively) than in the W(IV) precursor **4** (210 ppm), while all species have similar $^{1}J(^{13}C_{NHC}\text{-}^{183}W)$ coupling constants of ~140 Hz. In comparison to the methylidyne's carbon in **3** (302 ppm), the methylidene's carbon nuclei in **1** (283 ppm) and **2** (277 ppm) resonate up-field. Moreover, **1** (166 Hz) and **2** (148 Hz) show reduced $^{1}J(^{183}W\text{–}^{13}C_{CH2/CH})$ than **3** (221 Hz), in accord with the decreased W–C bond order and reduced *s*-character of the *sp²*-hybridyzed methylidene carbon. In addition to the standard set of data, taking advantage of ^{2}J couplings between proton/s at the methylidyne/dene ligands and ^{183}W, we collected 2D $^{1}H\text{–}^{183}W$ HMBC spectra and extracted isotropic chemical shifts for ^{183}W in high-valent W(VI) species.[76-78] Similar measurements for the W(IV) complex **1** were unfruitful due to the absence of *J*-couplings of adequate strength. The ^{183}W in the oxo-methylidyne **3** resonates at 405 ppm, which is in the range measured for highly Lewis-acidic tripodal W–carbyne complexes within three siloxide or fluorinated alkoxide ligands.[76] The ^{183}W resonance is shifted to 1332 ppm in the cationic oxo-methylidene **1**, and to 965 ppm in the neutral oxo-methylidene **2**. The different trends in ^{183}W and ^{13}C isotropic chemical shifts hint at more complex relations to electronic structure and motivates further in-depth analysis of chemical shift tensors based on solid-state NMR techniques.

Extracting NMR parameters from solid-state NMR.

Preamble. We turned to solid-state NMR spectroscopy in order to develop a detailed understanding of the relations between chemical shifts and electronic structures and further describe the olefin-coordination step in the olefin metathesis reaction. Solid-state NMR measurements enable extraction of the three principal components of the chemical shift tensor (CST) - δ_{11}, δ_{22} and δ_{33} ($\delta_{11} > \delta_{22} > \delta_{33}$ in ppm), the average of which corresponds to the isotropic chemical shift (δ_{iso}) observed in solution NMR measurements (eq. 1). The span ($\Omega = \delta_{11} - \delta_{33}$) and skew ($\kappa = 3(\delta_{22}-\delta_{iso})/\Omega$; $-1 \leq \kappa \leq 1$) values obtained from the CSTs conveniently describe solid-state NMR line-shapes and already provide information about the hybridization of the observed nuclei.[79] Computational orbital analysis of the three principal components, which are strongly tied to the three-dimensional electronic structure around the nuclei, can help to construct a detailed picture of frontier molecular orbitals (eq. 2 – 4). While the chemical shift (δ) can be experimentally observed and is defined with respect to a reference compound, chemical shielding (σ) is an intrinsic signature of the nuclei in a given environment and can be calculated. Therefore, the experimentally available CST values are used to validate the corresponding computed shielding tensor ($\sigma_{11} < \sigma_{22} < \sigma_{33}$) and access the electronic structure.[80] Chemical shielding values can be decomposed into (*i*) the diamagnetic contribution (σ_{dia}) that originates from the shielding of the nuclei by a "spherical" distribution of (mostly core) electrons, and typically remains constant across a range of related structures; (*ii*) the paramagnetic contribution that originates from external magnetic field-induced currents that are generated via the symmetry allowed couplings of occupied and empty frontier molecular orbitals (σ_{para}); as well as (*iii*) a contribution from the spin-orbit coupling (σ_{SO}) (eq. 3). The paramagnetic contribution to the (de-)shielding can be evaluated according to the Ramsey equation, that shows that frontier molecular orbitals of suitable symmetry that are close in energy are the major contributors to the chemical shift (eq. 4).[81] In other words, highly deshielded chemical shift principal component δ_{ii} (or the corresponding shielding component σ_{ii}) along a specific axis implies the presence of pair of occupied and vacant frontier orbitals close in energy and orthogonal to each other as well as the specific axis of the applied magnetic field.[80] Natural Chemical Shielding (NCS) analysis helps to reveal Natural Localized Molecular Orbitals (NLMOs) that contribute to each component of the shielding tensor (see the ESI for the detailed analysis).[80, 82-83]

$$\delta_{iso} = \frac{1}{3}(\delta_{11} + \delta_{22} + \delta_{33}) \quad (1)$$

$$\delta_{ii} = \sigma_{iso}^{ref} - \sigma_{ii}\ (i = 1, 2 \text{ or } 3) \quad (2)$$

$$\sigma = \sigma_{dia} + \sigma_{para} + \sigma_{SO} \quad (3)$$

$$\sigma_{para,ij} \Leftrightarrow -\frac{1}{2c^2}\sum_n \sum_k \frac{1}{E_n - E_0} \langle \Psi_0 | \hat{L}_{k,i} | \Psi_n \rangle \left\langle \Psi_n \left| \frac{\hat{L}_{k,j}}{r_k^3} \right| \Psi_0 \right\rangle \quad (4)$$

***Determination of experimental* ^{13}C *NMR parameters*:** solid-state ^{13}C NMR spectra of ^{13}C-enriched **1-^{13}C**, **2-^{13}C**, and **3-^{13}C** were collected at various spinning rates to unambiguously extract their NMR parameters (Figure 3 and S36-S38). The isotropic chemical shifts for ^{13}C nuclei of methylidene and methylidyne ligands determined from the solid-state NMR measurements agree well with the values determined from solution measurements (283, 274 and 298 ppm for **1**, **2**, and **3** in solutions, *vs.* 281, 277, and 302 for **1-^{13}C**, **2-^{13}C**, and **3-^{13}C** in solid-state). Complex **1** exhibits a signature typical for alkylidene species, *i.e.* a large span (Ω = 504 ppm) and a negative skew value (κ = −0.88).[25] The neutral oxo-methylidene complex **2** also exhibits similar ^{13}C solid-state NMR signature, however with an appreciably higher skew value (κ = −0.46) that is unusual for group 6 alkylidenes.[26]

The solid-state ^{13}C NMR spectrum of the oxo-methylidyne complex **3** contains two main and additional minor components with similar NMR parameters. This reflects the highly disordered nature of crystalline **3** having multiple structures with slightly different parameters (see the discussion on structural analysis in ESI; a single species is in fact detected in solution-state NMR experiments). The obtained line shape of **3** exhibits an unusual signature for an alkylidyne complex: while having a highly deshielded δ_{11} as commonly observed for alkylidynes, δ_{22} is significantly shielded yielding low skew values of −0.14 and −0.22 for the two main components. Such negative skew values are indeed closer to that for an sp^2-carbon ($\kappa << 0$) rather than for an expected *sp*-carbon ($\kappa \approx 1$) commonly determined for alkynes and transition metal alkylidyne complexes.[27, 84]

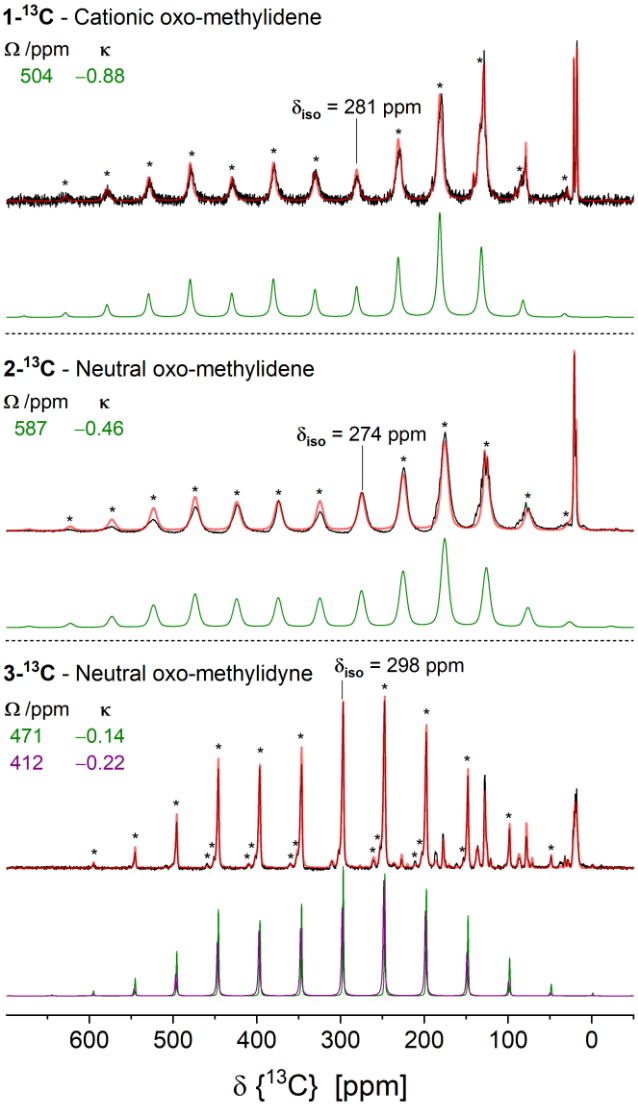

Figure 3. Solid-state ^{13}C CP-MAS (5 kHz) NMR spectra collected at room temperature (in black) and simulated traces (in red), with the main components (in green and purple) originating from ^{13}C-labeled methylidene/dyne ligands in cationic oxo-methylidene **1-^{13}C**, neutral oxo-methylidene **2-^{13}C**, and oxo-methylidyne **3-^{13}C**. The isotropic signal is marked with a line, spinning sidebands are marked with asterisks. Fitting parameters are validated by measurements at 16 or 20 kHz MAS (Figures S36-S38).

Determination of experimental ^{183}W NMR parameters: Solid-state ^{183}W NMR analyses have previously been extremely limited, mostly to W oxide materials. Recently, low temperature ^{183}W CP-MAS techniques were shown to enhance spectral sensitivity and provide access to ^{183}W NMR parameters,[85] which serve as a highly resolved probe of local structure of W atoms and were extended here to organometallic complexes **1** – **3**. Measurements at two spinning rates validate the extracted ^{183}W NMR parameters (Figure 4 and S39-S41). Two species with close parameters were identified in the spectra of both **1** and **2**, which are attributed to possible polymorphism in the powdered samples. For the following discussion, averaged parameters are analyzed. Cationic methylidene complex **1** shows the most deshielded signal ($\delta_{iso}(^{183}W)$ = 1327 ppm) with a broad span (Ω = 2843 ppm) and a slightly negative skew value (κ = −0.07). The neutral methylidene **2**, on the other hand, exhibits a more shielded spectrum ($\delta_{iso}(^{183}W)$ = 840 ppm) with appreciably reduced span (Ω = 1757 ppm) and skew value (κ = −0.38). Among the series, the methylidyne complex **3** exhibits the most shielded signals ($\delta_{iso}(^{183}W)$ = 254 ppm) with broad span (Ω = 2512 ppm) and slightly positive skew-value (κ = 0.09). The solid-state NMR δ_{iso} values match with solution $\delta_{iso}(^{183}W)$ values for methylidene species **1** and **2**, while for the methylidyne complex **3** it significantly departs from $\delta_{iso}(^{183}W)$ = 425 ppm detected in solution, indicating the substantial impact of dynamics. Overall, the cationic oxo-methylidene **1** and the oxo-methylidyne **3**, both with TBP geometry, reveal anisotropically broadened ^{183}W solid-state NMR spectra, while the neutral oxo-methylidene **2** with pseudo-octahedral geometry shows a more narrow spectrum with a distinctly negative skew-value.

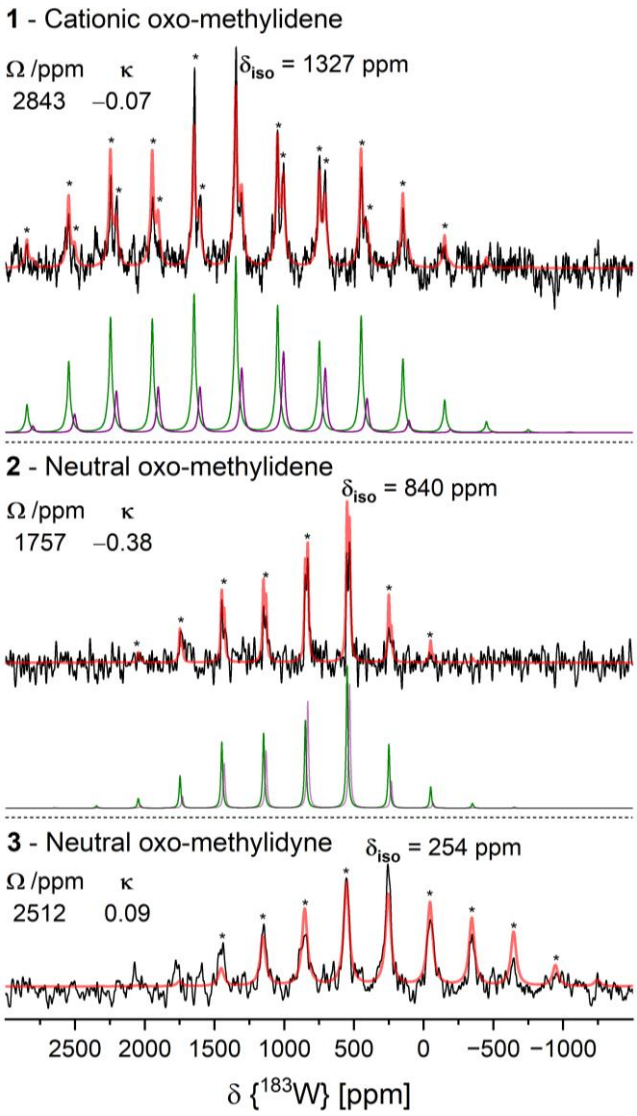

Figure 4. ^{183}W solid-state CP-MAS NMR spectra for **1** – **3** recorded at 94 K and 5 kHz MAS (black) and lineshape simulations (red). Spinning sidebands are marked with asterisks. Fitting parameters are validated by measurements at 8 kHz MAS (Figures S39-S41).

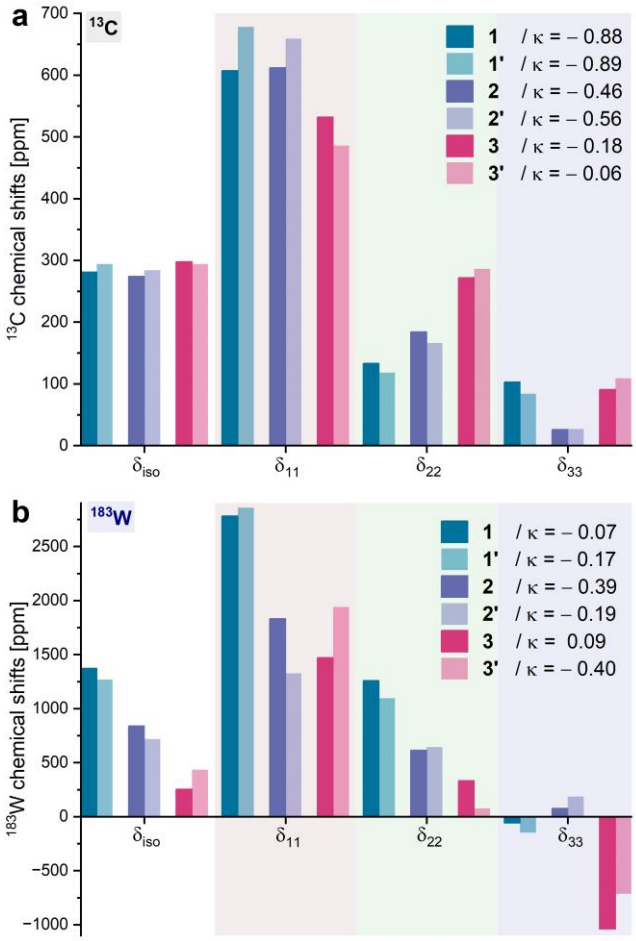

Figure 5. Extracted experimental solid-state (**a**) ^{13}C and (**b**) ^{183}W NMR parameters for **1** – **3** along with the calculated parameters for **1'** – **3'**.

Natural chemical shift analysis of NMR parameters.

Benchmarking calculations*:* In order to identify the specific orbital couplings that describe the observed NMR signatures, we carried out NCS analyses on each nucleus. Due to the very large systems studied here, we calculated NMR parameters for smaller models, derived from the scXRD structures, in which the mesityl moieties of NHC ligands were replaced by methyl groups. The truncated models are denoted **1'**, **2'**, and **3'**. Notably, the calculated ^{13}C CST parameters, and therefore δ_{iso}, for **1'** – **3'** are in excellent agreement with the experimentally obtained values (Figure 5a).[86] The computed ^{183}W NMR parameters also correlate well with measured values (R^2 = 0.93, Figures 5b and S42),[87-88] with a few deviating from the correlation line, in particular for the oxo-methylidyne pair **3**/**3'** (κ = 0.09 *vs.* −0.40 for **3** and **3'**, respectively). Close examination of the shielding components reveals that the varied contributions from spin-orbit term σ_{SO} (see eq. 3) causes the deviation of some components with respect to the experimental values (the influence of σ_{SO} on the principal components are summarized in Table S13). The σ_{SO} term, which is determined as a difference between the spin-orbit and scalar-relativistic level of calculations, contributes almost equally to all three principal components in complex **1'** yielding an excellent match with experimentally obtained parameters (*av.*(σ_{SO}) = 2322 ppm, Δ(σ_{SO}) = 19 ppm).

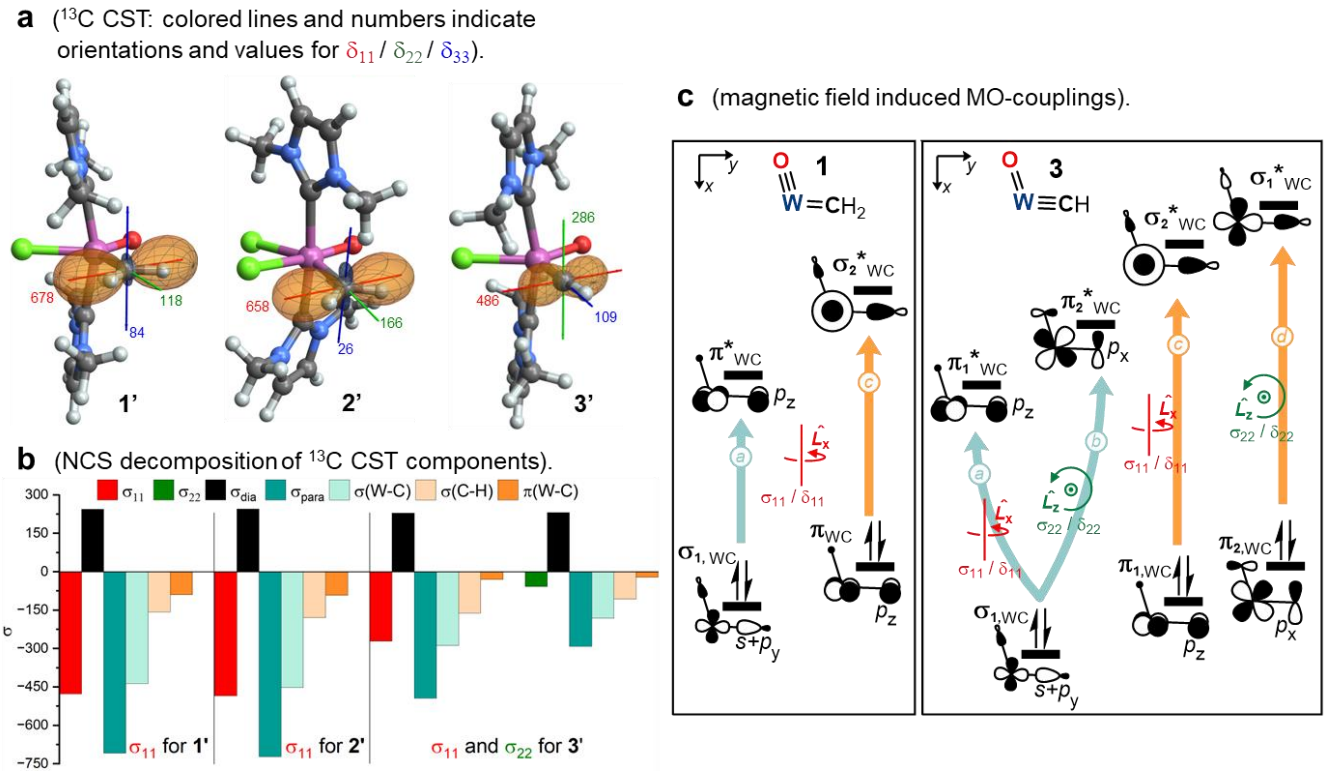

Figure 6. (**a**) Visualized [13]C CST orientations for **1'** – **3'**. Colored lines indicate orientations of principal components (δ_{11}, δ_{22}, δ_{33}), with chemical shift values given in ppm; (**b**) contribution of individual orbitals to methylidene/dyne ligands' [13]C σ_{11} in **1'** – **3'** and σ_{22} in **3'**; (**c**) the main orbital couplings (denoted as a, b, and c) contributing to σ_{11} in methylidene complexes and $\sigma_{11/22}$ in methylidyne

On the other hand, in **3'** the contribution of σ_{SO} term varies significantly between the three principal components. The σ_{SO} term contributes 2265 ppm and 2513 ppm to δ_{11} and δ_{22} respectively, driving the shielding in the direction of latter, and hence resulting in a more negative skew value than that for **3** determined experimentally. The same is also true for the deviation of δ_{11} in **2'**, for which higher σ_{SO} contribution drives shielding away from the values determined for **2**. Overall, despite these discrepancies, considering the broad chemical shift window for [183]W NMR, a good correspondence between the computed and experimental NMR parameters are obtained. These results, combined with the systematic structural variations in the series of complexes **1**, **2**, and **3** (and models **1'**, **2'**, and **3'**) provide ideal opportunity to assess the impact of geometry and ligand nature on NMR parameters.

Analysis of [13]C NMR parameters: We initiated our analysis with [13]C NMR signatures. To begin with, the visualized chemical shielding tensors (CSTs) are summarized in Figure 6a. The two alkylidene species **1'** and **2'** share a common orientation of their CSTs. The most deshielded component (δ_{11}) is perpendicular to the W–C_{CH2} axis, and lies on the molecular equatorial plane, while the second-most deshielded component (δ_{22}) is oriented along the W–C_{CH2} axis. The most shielded component (δ_{33}), by definition, is directed perpendicular to other two and points parallel to the C_{NHC}–W–C_{NHC} axis. Such orientation of CSTs agrees with reported alkylidene species.[25-27, 89] On the other hand, methylidyne **3'** has its δ_{11} and δ_{22} perpendicular to the W–C_{CH} bond; δ_{11} points parallel to the equatorial plane and δ_{22} is orthogonal to it, while δ_{33} points along the W–C_{CH} bond axis. Although such orientations are in agreement with reported alkylidyne complexes,[27, 90-92] the overall shape of the tensor with unusually low skew value ($\kappa = -0.06$), defined by unusually shielded δ_{22} component, implies developed sp^2-hybridized character ($\kappa << 0$) of the carbon atom rather than expected sp-hybridization ($\kappa \approx 1$).

To reveal the origin of the observed NMR signature and trends, we conducted NCS analysis. Among the series (**1'** – **3'**), the paramagnetic term (σ_{para}) drives chemical shifts, while the diamagnetic term (σ_{dia}) remains invariant. Therefore, orbital contributions to the σ_{para} of each principal component are analyzed (Figures 6b and S51-S53). In methylidene complexes **1'** and **2'**, the most deshielded component (δ_{11}) is primarily driven by the coupling of filled σ(W=C_{CH2}) orbital with low-lying, vacant π^*(W=C_{CH2}) orbital as expected for alkylidene ligands (Figure 6c, left, coupling a).[25-27] The major difference in spectral signatures between **1/1'** and **2/2'** pairs stems from the more deshielded δ_{22} component for the latter; this originates from the enhanced contribution from σ(C–H), that is coupled with the π^*(W=C_{CH2}) orbital, in **2'** than in **1'** (Figures S51 and S52). This is likely related to the longer W–C_{CH2} bond distance in **2/2'** than in **1/1'** (see above), due to the trans influence of the chloride ligand in an octahedral complex. Consequently, the complex **2** may feature a less destabilized π^*(W=C_{CH2}) orbital that is better coupled with the σ(C–H) orbital yielding a more deshielded δ_{22} and resulting in an overall distinct line shape from **1**. The oxo-methylidyne complex and model **3/3'** feature unusually distinct δ_{11} and δ_{22} values, which hints at the considerable sp^2-nature of the alkylidyne fragment. NCS analysis suggests that the dominant contribution in δ_{11} and δ_{22} originate from the coupling of

filled σ(W≡C_{CH}) orbital with two orthogonal π*(W≡C_{CH}) orbitals, with higher contribution in δ_{11} than in δ_{22} (Figure 6c, right, couplings *a* and *b*).[90] As these two couplings share the same filled orbital at their origin, the different degree of destabilization of two empty π*(W≡C_{CH}) orbitals must cause drastically distinct contributions to δ_{11} and δ_{22} . Combined with the orientation of the CST, the larger deshielding of δ_{11} than δ_{22} suggests that the *out-of-plane* π_1*(W≡C_{CH}) orbital, along the C_{NHC}–W–C_{NHC} axis, is lower in energy than the *in-plane* π_2*(W≡C_{CH}) orbital yielding better coupling with the former (Figure 6c, right). This difference in the two π-orbitals originates from the presence of the additional π-donating oxo-ligand, which can be referred to as a "π-loading effect".[93-95] While one of the p-orbitals of the methylidyne carbon forms a fully developed π-bonding along the C_{NHC}–W–C_{NHC} axis (*out-of-plane*), the second *in-plane* carbon p-orbital shares the same tungsten d-orbital with the oxo ligand (orbital $\pi_{2,WC}$ in Figure 6c).[96-97] This orbital-competition results in the less developed *in-plane* π(W–C_{CH}) orbital, rendering the methylidyne ligand with partial alkylidenic character, *i.e.* sp^2- hybridization.

Overall, the analysis of ^{13}C solid-state NMR data reveals the detailed picture of W–C multiple bonding, addressing the influence of additional σ- and π-donor ligands. The obtained description agrees well with scXRD molecular structures that show complementing variations in W–$C_{CH2/CH}$ and W–O bond distances.

Analysis of calculated ^{17}O NMR parameters: To further substantiate the interplay between basal ligands, we calculated and analyzed ^{17}O NMR parameters of the oxo ligands in **1'** – **3'** (Figure 7a).[28-29, 98] The calculated ^{17}O NMR parameters and the resulting line shapes vary significantly in the series. Notably, **1'** features a highly shielded δ_{22} and therefore low skew value (κ = 0.19) which is unexpected for a group 6 oxo species.[28-29] For instance, **2'** has a calculated skew value of 0.79 indicating the axially symmetric, *sp*-hybridized, oxo ligand in line with previous studies on tetrahedral Schrock-type alkylidenes.[28] The model **3'** features an even further lowered skew value of −0.25, pointing to its primarily sp^2-hybridized oxo ligand.

Visualized ^{17}O CSTs of each complex show δ_{11} oriented perpendicular to the W–O bond axis and laying on the equatorial plane. Models **1'** and **2'** reveal their δ_{22} oriented parallel to the C_{NHC}–W–C_{NHC} axis, while δ_{33} pointing along the W–O bond axis analogously to the *sp*-hybridized carbon atoms. In comparison to **1'** and **2'**, in the model **3'**, δ_{22} and δ_{33} switch positions and orient similarly as ^{13}C principal components in sp^2-hybridized alkylidenes (*cf.* Figure 7b for ^{17}O and Figure 6a for ^{13}C). Overall, these orientations suggest an *sp*-hybridized oxo ligand for **1'** and **2'**, and sp^2-oxo for **3'**, complementing the above discussion on ^{13}C NMR signatures.

The unusually low ^{17}O skew value in **1'** is caused by the compromised π(W–O) bond originating from the orbital-competition, analogous to the above discussion on the methylidyne ligand of **3'**, though in this case with the chloride ligand. In a TBP geometry, the σ(W–Cl) bonding competes for the metal d-orbital that is involved in the *in-plane* π(W–O) bonding (Figure 7c), thus reducing the π-bonding around oxo ligand, hence its sp^2 character. This contrasts with pseudo-octahedral **2'** lacking such an orbital competition, and thus featuring an oxo ligand with fully developed W–O triple bonding as suggested by its skew values close to 1. In **3'**, the *in-plane* π(W–O) bonding is further lost in favor for the *in-plane* π(W–C_{CH}) bonding with the methylidyne ligand in addition to the σ(W–Cl) bonding; this results in the dominant sp^2-nature of its oxo moiety. Altogether, in analogy with the discussion on ^{13}C skew values (*vide supra*), the calculated ^{17}O NMR parameters indicate a *sp*-hybridized and triply bonded oxo-ligand in **2'**, and a primarily sp^2-hybridized and doubly bonded oxo ligand in **3'**. Accordingly, the nature of the oxo-ligand in **1'** – *sp*-hybridized, however with considerable sp^2-character – is in between those in **2'** and **3'** (Figure 7d). These overall assignments are, in fact, complementary to the hybridization around methylidene/dyne fragments.

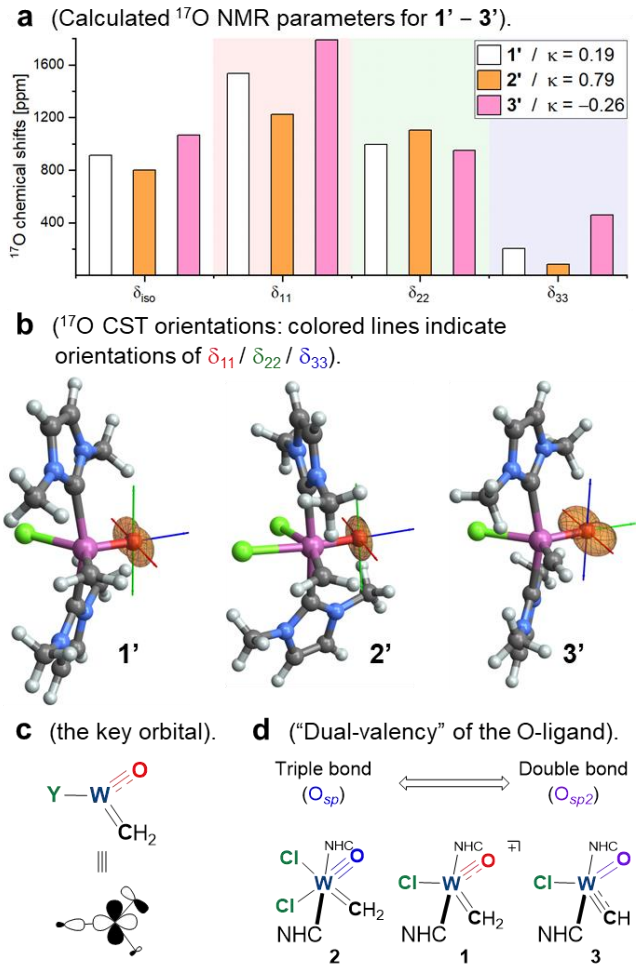

Figure 7. (**a**) Calculated ^{17}O CSA pattern for **1' – 3'**; and (**b**) their ^{17}O CST orientations; (**c**) the key interaction between three basal ligands of the TBP oxo-alkylidene complex; (**d**) illustration of the dual-valency of the oxo ligand in the series of complexes.

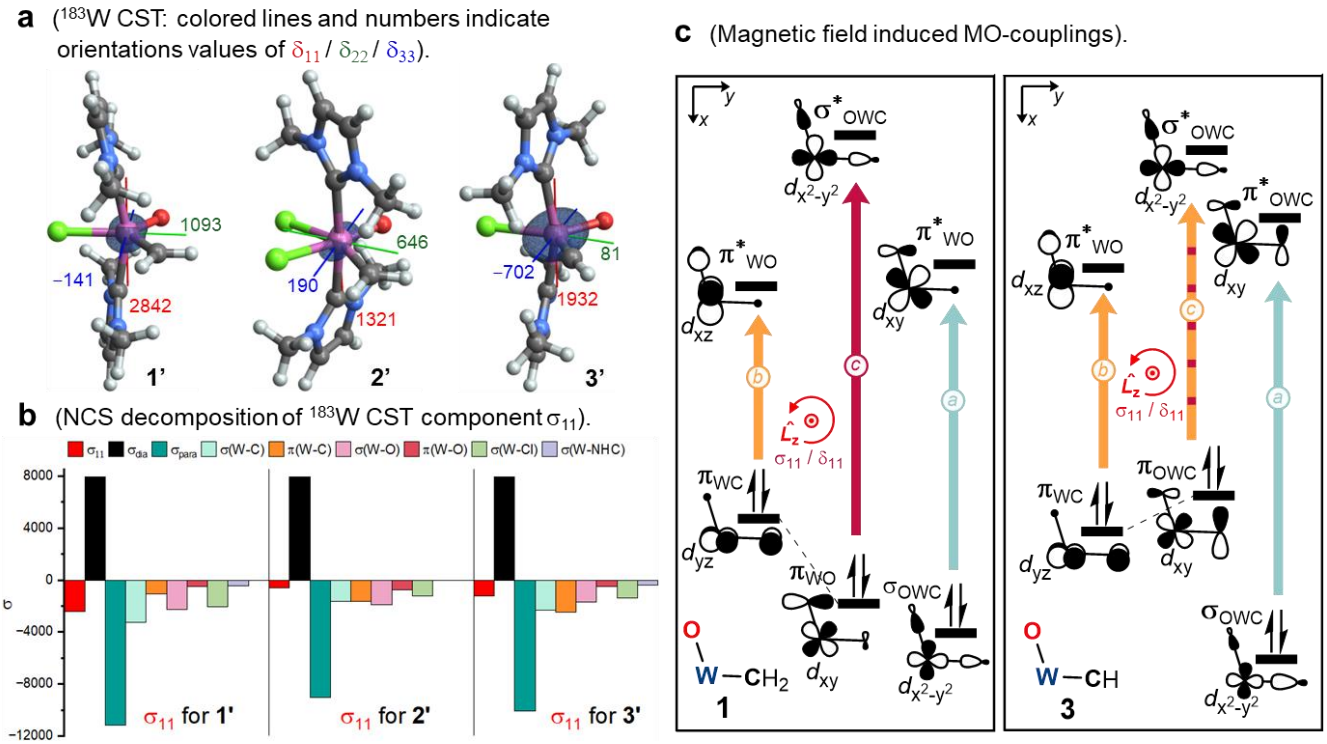

Figure 8. (a) Visualized ^{183}W CST orientations for **1'** – **3'**. Colored lines indicate orientations of principal components (δ_{11}, δ_{22}, δ_{33}) for ^{183}W, with chemical shift values given in ppm; (b) contribution of individual orbitals to ^{183}W σ_{11} in **1'** – **3'**; (c) the main orbital couplings contributing to σ_{11} of central ^{183}W nuclei.

Analysis of ^{183}W NMR parameters: Finally, ^{183}W NMR parameters were analyzed to gain an overview of the interplay between the σ - and π-donor ligands at the metal site. The ^{183}W CSTs of **1'** – **3'** are oriented similarly (Figure 8a) with δ_{11} directed along the C_{NHC}–W–C_{NHC} axis, δ_{22} bisecting the O–W–$C_{CH/CH2}$ bond angle, while δ_{33} is orthogonal to other two axes crossing between the chloride(s) and other two basal ligands. Based on these orientations, the following discussion focuses on the σ_{11} components not only because it is the most driven by structural variations, but also because it is orthogonal to the molecular basal plane. The rotation around this specific axis "operates" on the orbitals relevant to alkylidene/dyne, oxo, and chloride ligands. With this in mind, we conducted NCS analysis on the paramagnetic term in the three complexes, revealing the NLMO contributions (Figure 8b for σ_{11} and Figures S54–S56 for σ_{22} and σ_{33}). Pertinent to this discussion, relevant orbital couplings for **1'** and **3'** are illustrated in Figure 8c. The model **1'** features generally high contributions from σ-type orbitals, which arises from the cationic nature of **1'** with low-lying vacant orbitals, facilitating better couplings. Comparison between **1'** and **2'** points out the impact of geometry: σ_{11} acquires higher contributions from σ-type orbitals in **1'**, while contributions from π-type orbitals are higher in **2'**. These could be rationalized taking into account the following differences between TBP (**1'**) and quasi-octahedral (**2'**) geometries: (*i*) d_{x2-y2}-derived σ-type bonding orbital contributes more in TBP geometry (*i.e.* **1'** > **2'**) to deshielding, as it is further stabilized in octahedral environment resulting in a larger energy gap in the latter; (*ii*) d_{xz} and d_{yz}-derived π-type orbitals contribute more in octahedral structures (*i.e.* **2'** > **1'**) due to improved spatial overlap with π*-orbitals upon 90 ° rotation with the effect of rotation operator.

The additional π(WC) bond in TBP methylidyne complex **3'** further modulates the relevant orbitals and NMR signature, featuring reduced contributions from σ-type orbitals and increased contribution from π(WC) orbitals when compared to TBP **1'** (Figure 8c, right). The reduced contribution from σ-type orbitals in **3'**, originates from the increased energy gap between two coupling partners (denoted as coupling a): the σ(OWC) orbital is stabilized due to the more electronegative *sp*-hybridized methylidyne ligand, and *in-plane* π*(OWC) orbital is destabilized due to the antibonding interaction with both oxo and methylidyne ligands. More than twice higher contribution from two π(WC) in **3'** *vs.* **1'** reflects the change in nature of the d_{xy}-derived *in-plane* π-bonding orbital from low-lying π(WO) character in **1'** to high energy π(WC) character in **3'**. Overall, NCS analysis of the σ_{11} principal component of ^{183}W CSTs evidences the effect of geometry (**1'** *vs.* **2'**) and ligand nature (**1'** *vs.* **3'**) on NMR parameters. This analysis further highlights the competition between oxo and methylidene/dyne ligands as illustrated in their varied degree of contribution of σ(OWC), π(WC), and π(WO) NLMOs to the deshielding of σ_{11} (Figure 8c). Notably, the outcome of NCS analysis on ^{183}W CST agrees with and extends the description obtained from the analysis of ligand-based ^{13}C and ^{17}O NMR parameters, highlighting the strength of ^{183}W NMR in enabling direct access to the metal-centered electronic structure.

To summarize, the analysis based on experimentally obtained structural data as well as solid-state NMR data on multiple nuclei points out the unique bonding situation in TBP **1/1'** featuring an oxo ligand with significant sp^2-nature, which was

further corroborated in comparison with the closely related **2/2'** and **3/3'**. The interplay among basal ligands, competing for the same metal d-orbital, compromises multiple bonding with the oxo and methylidyne ligands. Importantly, in TBP complexes, chloride (*i.e.* anionic σ-donor) ligand-induced loss of multiple metal-oxo bonding can also have a place in olefin-coordination intermediates of Chauvin cycle (*vide infra*).

DISCUSSION

Relating the electronic structures of surrogate and metathesis-active olefin intermediate.

With the discussion above in hand, we explore whether this analysis, especially on **1'**, can be transferred to the closely related TBP olefin-coordination intermediate of the metathesis cycle. Following the study of the surrogate complexes **1/1'**, we modeled the olefin-coordination intermediate $\mathbf{Int_{Cl}}$ featuring a coordinated ethylene ligand in place of one of the NHC ligands (see ESI for details) and examined its NMR signatures and associated electronic structures (Figure 9). The calculated ^{13}C NMR parameters of $\mathbf{Int_{Cl}}$ agree well with those of **1'** (Figure 9a). The obtained ^{13}C CST for $\mathbf{Int_{Cl}}$ features skew value of −0.82, close to that of **1'** (κ = −0.89), which is typical for *sp*^{2}-hybridized carbenes in Schrock-type alkylidenes. The ^{13}C nucleus of the methylidene ligand in $\mathbf{Int_{Cl}}$ has a δ_{iso} of 335 ppm, which is slightly deshielded compared to that found for **1'** (δ_{iso} = 294). This difference is mainly driven by the more deshielded δ_{11} in $\mathbf{Int_{Cl}}$ (δ_{11} = 772 ppm) compared to **1'** (δ_{11} = 678 ppm). The larger deshielding in $\mathbf{Int_{Cl}}$ implies the presence of high-energy occupied π(W=C), as well as low energy vacant π*(W=C) orbitals. Indeed, the corresponding FMOs relevant to deshielding show stabilized bonding combination of π*(W=C) with low-lying π*(C=C) orbital of ethylene in $\mathbf{Int_{Cl}}$ (Figure 9b). Likewise, the occupied π(W=C) orbital in $\mathbf{Int_{Cl}}$ is also destabilized by symmetry matching π(C=C) orbital of ethylene, which again drives deshielding of δ_{11} compared to NHC-coordinated **1'** (Table S14). Overall, the calculated ^{13}C NMR parameters for $\mathbf{Int_{Cl}}$ match well those for surrogates **1/1'** with deviations that originate from the different orientations of π-orbitals of ethylene and NHC ligands.

The calculated isotropic ^{183}W chemical shift for $\mathbf{Int_{Cl}}$ (δ_{iso} = 1282 ppm) closely matches that for **1'** (1265 ppm) with only 17 ppm difference in the vast (> 10,000 ppm) chemical shift window of ^{183}W NMR (Figure 9c). Moreover, their ^{183}W CSTs are oriented similarly, permitting direct comparison of each principal component between two models (Figure 9d). Respective CST components of $\mathbf{Int_{Cl}}$ indeed corresponds to those for **1'** reasonably well, indicating that the **1/1'** pair are valid electronic surrogates of the olefin-coordination intermediate $\mathbf{Int_{Cl}}$. Among the CST components of **1'** and $\mathbf{Int_{Cl}}$, the largest deviation of 483 ppm is found in δ_{22}, resulting in a significantly lower skew value for the latter (κ = −0.17 and −0.62 for **1'** and $\mathbf{Int_{Cl}}$, respectively). This difference is independent of the spin-orbit coupling (σ_{SO} term contribution in δ_{22} is 2330 ppm for **1'** and 2370 ppm for $\mathbf{Int_{Cl}}$) and originates from the reduced contributions to δ_{22} from the σ(W–C_2H_4) NLMO in $\mathbf{Int_{Cl}}$ compared to the original σ(W–C_{NHC}) orbital in **1'** (Table S18). On the other hand, the δ_{11} parameter along the NHC–W–L is least affected by the substitution of NHC to ethylene, which implies that the discussion around δ_{11}, based on **1/1'** (*vide supra*), can be directly transferred to $\mathbf{Int_{Cl}}$. The ^{17}O NMR parameters of the oxo ligand in $\mathbf{Int_{Cl}}$ also match with those for **1'** with a skew value of 0.09 (*cf.* κ(^{17}O) = 0.16 for **1'**), showing that the TBP olefin-coordination intermediate complex must also feature an oxo-ligand with increased *sp*^{2}-character (Table S10). This scenario stands in sharp contrast to what has been previously shown for tetrahedral oxo-alkylidenes and TBP metallacyclobutane intermediates, for which the NMR analysis suggests fully developed M–O triple bonding.[28] Overall, the comparison of the calculated ^{13}C, ^{17}O and ^{183}W NMR parameters on **1/1'** with the olefin intermediate $\mathbf{Int_{Cl}}$ yielded congruence in each nucleus, validating our approach with surrogate complexes to access the electronic structure of the elusive olefin-coordination intermediate. Observed deviations in ^{13}C and ^{183}W NMR parameters were found to arise from inherent differences between NHC and ethylene ligands, which have their π-systems in orthogonal directions. While the olefin-coordinated TBP intermediate features typical alkylidene character, its oxo fragment exhibits significant *sp*^{2}-character with *in-plane* π-bonding compromised with the σ-donation from the chloride ligand, motivating further analysis of the role of the Y-ligand.

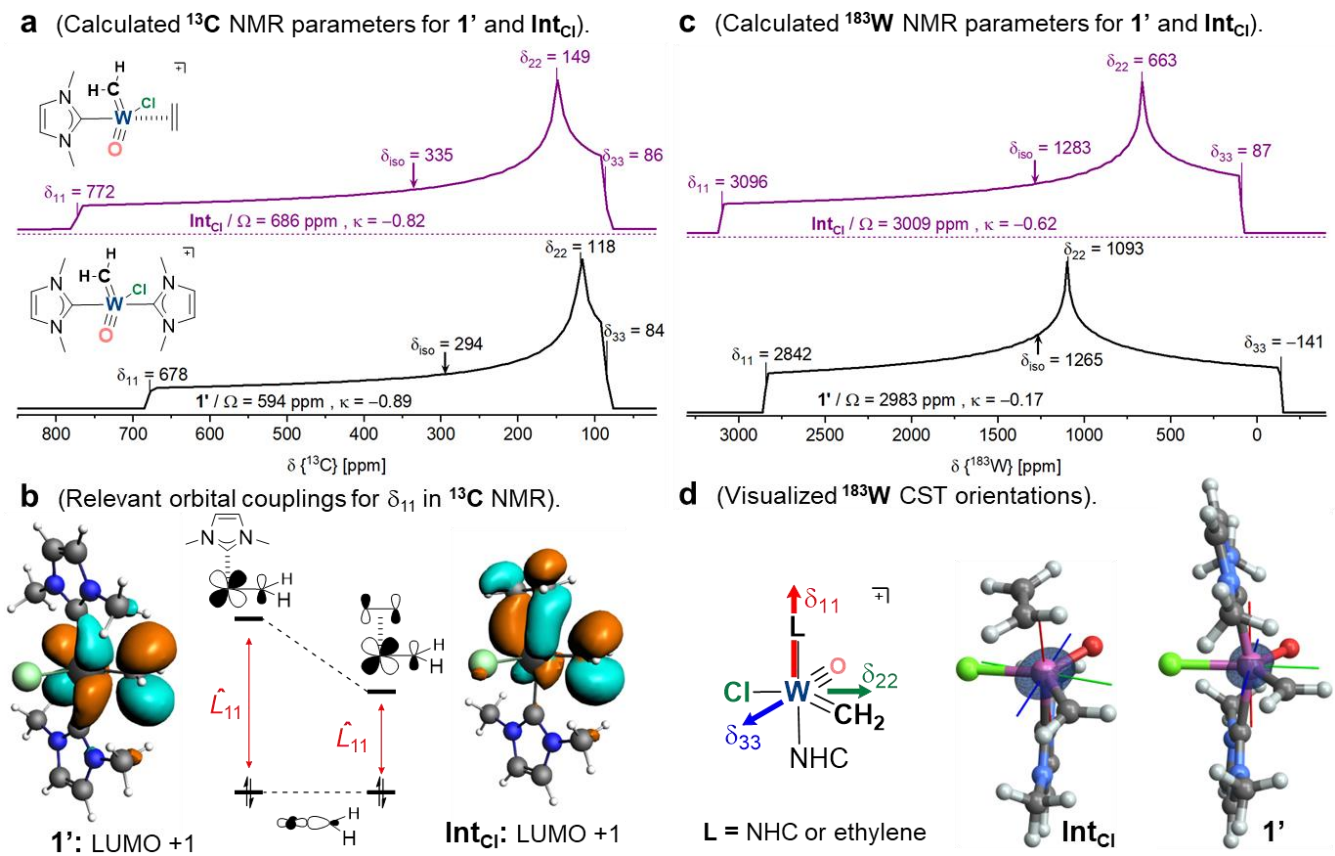

Figure 9. (**a**) The comparison of ^{13}C CSA patterns for **1'** and **Int$_{Cl}$**. (**b**) the relevant orbital couplings contributing to ^{13}C σ_{11} of the methylidene ligand in **1'** and **Int$_{Cl}$**, along with the key LUMO+1 orbitals for both complexes. (**c**) The comparison of ^{183}W CSA patterns for **1'** and **Int$_{Cl}$**; and (**d**) their visualized ^{183}W CST orientation.

Effect of Y-ligand on olefin metathesis catalysis and origin of "weak σ-donor" preference.

The discussion above has highlighted the unique electronic structure of TBP olefin intermediate **Int$_{Cl}$** (or its surrogates **1** and **1'**), pointing out that the olefin coordination induces a major change of hybridization of the oxo ligand, from *sp* towards *sp*^{2}, as a result of the competition between the σ-donating Y-ligand and the *in-plane* p-orbital of the oxo ligand for a single d-orbital of the central metal. This parallels the proposition by Rappé and Goddard on the dual valency of the oxo ligand in olefin metathesis, and the established activity patterns of metathesis catalysts.[99-101] It has been shown that the coordination of olefin onto alkylidenes, and concomitant structural reorganization to TBP geometry, is often rate determining in Schrock-type catalysts [M(=CHR)(E)(X)(Y)] where the energy barrier greatly depends on the σ-donating capacity of the Y-ligand: the weaker σ-donor, the lower the barrier.[18-22] Such reactivity pattern implies that the re-hybridization around the oxo ligand, enhanced by a σ-donating Y-ligand, is likely a key factor that determines the olefin-coordination barrier. Therefore, we modeled a series of complexes **Int$_Y$** with Y ligands of distinct σ-donating character (Y = Me, Cl, O^{t}Bu and O^{t}Bu-F$_9$, in increasing σ-donating capacity), while keeping the rest of the structure intact, and analyzed their ^{13}C, ^{17}O and ^{183}W NMR parameters (Tables S9–S10). Calculated ^{17}O skew values for oxo ligands showed systematic increase in the order of **Int$_{Me}$** (κ = −0.25) < **Int$_{Cl}$** (κ = 0.09) < **Int$_{OtBu}$** (κ = 0.23) < **Int$_{OtBu\text{-}F9}$** (κ = 0.36) (Table S10). The negative skew value (κ = −0.25 comparable to that in **3'**) for the oxo ligand in **Int$_{Me}$** suggests its primarily *sp*^{2}-nature, while more positive skew values in **Int$_{OtBu}$** and **Int $_{OtBu\text{-}F9}$** point to an *sp*-hybridization. This trend in NMR response suggests more *sp*-hybridized oxo ligand in the presence of weaker σ-donor Y ligand, and vice versa, which perfectly follows the established Schrock-type catalyst design principles that favor weakly donating Y-ligand such as alkoxides or fluorinated alkoxides, rather than alkyls.[14-15, 102]

The influence of Y-ligand substitution is even more evident in the calculated ^{183}W NMR signatures of **Int$_Y$** series (Figure 10, Table S12). While δ_{22} and δ_{33} show minor deviations within the series, δ_{11} shifts over 2800 ppm (**Int$_{Me}$ > Int$_{Cl}$ > Int$_{OtBu}$ > Int$_{OtBu\text{-}F9}$**) in the order complementary to those for ^{17}O NMR parameters. According to the NCS analysis on δ_{11}, the contribution from the σ(W–Y) orbital drives this change (Table S17). Furthermore, the inspection of the σ(W–Y) NLMOs revealed increased W-based orbital contribution with more electron donating ligands (*i.e.* covalent bond) (Figure S50). Hence, as illustrated in Figure 11, in contrast to a weak σ-donor ligand such as (F$_9$)-*tert*-butoxy, a stronger σ-donating ligand will lead to high-energy and more covalent σ(W–Y) interaction having higher localization on W; both of these factors drive deshielding due to the resulting smaller energy gap and larger spatial overlap with the coupled vacant orbital.

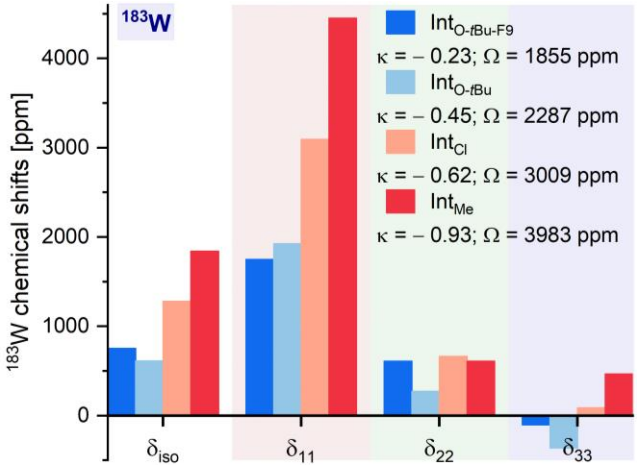

Figure 10. Summary of the calculated ^{183}W NMR parameters for a series of olefin-coordination intermediates **Int$_Y$**.

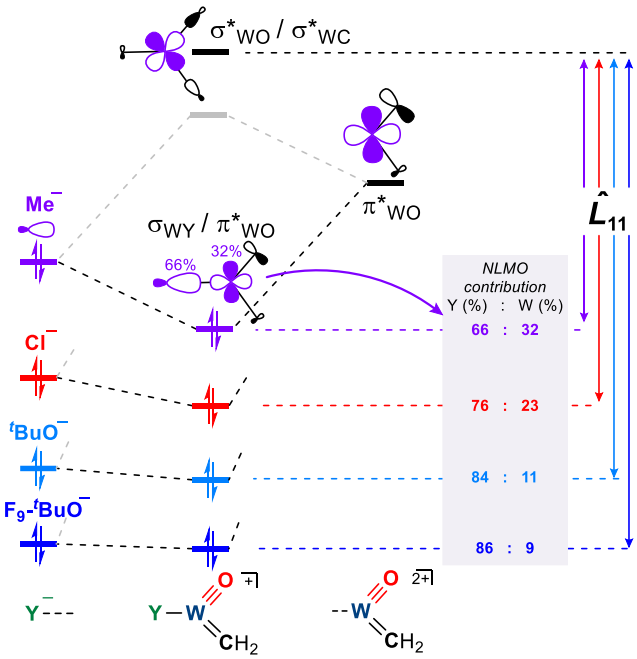

Figure 11. Qualitative MO diagram for **Int$_Y$** models. The degree of ^{183}W δ_{11} deshielding is rationalized based on energy gap between two coupling orbitals, and the degree of covalency of the σ(W-Y) bonding.

Overall, ^{17}O and ^{183}W NMR parameters suggest that strongly donating Y-ligands (such as alkyl) bond more covalently with the central metal impairing the *in-plane* π-bonding with the oxo ligand, and thus favoring its *sp*^{2}-hybridization. The need for a weakly donating Y ligand herein becomes evident, as it does not induce considerable E-ligand (oxo herein) re-hybridization during the olefin coordination step. Accordingly, some types of E ligands will tolerate strongly donating Y-ligands due to additional mechanisms favoring rehybridization. Not surprisingly, highly efficient Schrock-type catalysts usually feature aryl-imido (E = N–Ar) instead of alkyl-imido (E = N–Alkyl) ligands due to the lower donating capacity of former rendering the loss of triple bonding upon olefin coordination energetically less expensive.[16, 103-105] On the other hand, for alkylidyne ligands (E = C–R) on Re-based catalysts, re-hybridization is barely available and having a weakly donating Y-ligand is paramount for catalysis.[19] Hence, rhenium alkylidyne based catalyst performs well only when grafted to silica – a "ligand" with small σ-donation.[106]

CONCLUSION

Aiming at developing a molecular surrogate for elusive olefin-coordinated alkylidene intermediate in olefin metathesis reaction, we have developed NHC-stabilized cationic W oxo-methylidene complex **1**, along with the neutral oxo-methylidene complex **2** and the oxo-methylidyne analog **3**. Analysis of the experimental ^{13}C and ^{183}W solid-state NMR signatures as well as computational ^{17}O NMR parameters for the oxo ligand on these compounds helps to reconstruct and understand their electronic structures. Notably, analysis of the NMR parameters highlights the competition between the various ligands bound to W, modulating the hybridizations of the oxo (E) ligand. Analysis of the corresponding olefin-coordination complex model $\mathbf{Int_{Cl}}$ shows that NHC and olefin have similar effects on the NMR signatures, supporting high sp^2-character of the oxo ligand in this intermediate. The degree of the re-hybridization of the oxo ligand to sp^2 (from *sp* in the starting alkylidene and further in metallacyclobutane) correlates with the σ-donating capacity of the Y ligand as the oxo and Y ligands compete for the same tungsten d-orbital in a TBP olefin-coordination intermediate. This change of hybridization parallels the known catalytic activity trends for Schrock-type alkylidenes and supports the hypothesis on "dual-valency" of the oxo ligand raised by Rappé and Goddard. Calculated metal and ligand NMR parameters of hypothesized intermediates could thus be a facile way to rapidly screen candidate of metathesis catalysts *in silico*. This work further demonstrates that along with conventionally used ligand-based NMR techniques, the analysis of the NMR response of the central metal, herein ^{183}W, helps to analyze the overall effect of ligand sphere, and describe electronic structure anchored on experimental data. We are currently further exploring metal-based NMR to understand the electronic structure of catalysts with the ultimate goal to identify robust reactivity descriptors.[107]

ASSOCIATED CONTENT

Supporting Information

The supporting information is available free of charge at is available free of charge. General procedures and technical details; details of synthetic procedure, characterization, structural analysis, solution and solid-state NMR experiments and calculations.

Accession Codes

CCDC 2346348 – 2346351 contain the supplementary crystallographic data for this paper. These data can be obtained free of charge via www.ccdc.cam.ac.uk/data_request/cif, or by emailing data_request@ccdc.cam.ac.uk, or by contacting The Cambridge Crystallographic Data Centre, 12 Union Road, Cambridge CB2 1EZ, UK; fax: +44 1223 336033.

AUTHOR INFORMATION

Corresponding Authors

Christophe Copéret – *Department of Chemistry and Applied Biosciences, ETH Zürich, CH-8093 Zürich, Switzerland, https://orcid.org/0000-0001-9660-3890; Email:* ccoperet@ethz.ch

Sadig Aghazada – *Department of Chemistry and Applied Biosciences, ETH Zürich, CH-8093 Zürich, Switzerland, https://orcid.org/0000-0002-7568-4481; Email: sadig.aghazada@gmail.com*

Author

Yuya Kakiuchi – *Department of Chemistry and Applied Biosciences, ETH Zürich, CH-8093 Zürich, Switzerland, https://orcid.org/0000-0001-5882-2320.*

Scott R. Docherty – *Department of Chemistry and Applied Biosciences, ETH Zürich, CH-8093 Zürich, Switzerland, https://orcid.org/0000-0002-8605-3669.*

Zachariah J. Berkson – *Department of Chemistry and Applied Biosciences, ETH Zürich, CH-8093 Zürich, Switzerland, https://orcid.org/0000-0002-2157-4172.*

Alexander V. Yakimov – *Department of Chemistry and Applied Biosciences, ETH Zürich, CH-8093 Zürich, Switzerland, https://orcid.org/0000-0002-8624-1002.*

Michael Wörle – *Department of Chemistry and Applied Biosciences, ETH Zürich, CH-8093 Zürich, Switzerland, https://orcid.org/0000-0001-8087-5779.*

Notes

The authors declare no competing financial interest.

Funding Sources

S.A. acknowledges a fellowship from the Swiss National Science Foundation (grant number: P5R5PN_202658). C.C., S.R.D., and Y.K. acknowledge the Swiss National Science Foundation (grant numbers: 200021_169134, 200020_214994, and 200020B_192050). C.C. and A.V.Y. gratefully acknowledge ETH+ Project SynthMatLab for the financial support.

ACKNOWLEDGMENT

All simulations were performed on the ETH-Zürich Euler cluster. We thank Lukas Lätsch for the fruitful discussion. S.A. thanks Prof. Dominik Munz for valuable discussions on DFT calculations. We thank Dr. Darryl Nater for assistance with the XRD measurements. We gratefully acknowledge SwissCat+ for the usage of the LT MAS 400 MHz spectrometer.

ABBREVIATIONS

NMR, nuclear magnetic resonance; solid-state NMR, solid-state nuclear magnetic resonance; CST, chemical shielding tensor; CSA, chemical shift anisotropy; PC, principal component; MAS, magic angle spinning; δ, chemical shift; σ, chemical shielding; Ω, span; κ, skew; scXRD, single crystal X-ray diffraction; DFT, density functional theory; NCS, Natural chemical shielding; NLMO, natural localized molecular orbital; MO, molecular orbital; TBP, trigonal bipyramidal; NHC, N-heterocyclic carbene.

REFERENCES

1. Chauvin, Y., Olefin Metathesis: The Early Days (Nobel Lecture). *Angew. Chem. Int. Ed.* **2006,** *45* (23), 3740-3747.
2. Grubbs, R. H., Olefin-Metathesis Catalysts for the Preparation of Molecules and Materials (Nobel Lecture). *Angew. Chem. Int. Ed.* **2006,** *45* (23), 3760-3765.
3. Schrock, R. R., Multiple Metal–Carbon Bonds for Catalytic Metathesis Reactions (Nobel Lecture). *Angew. Chem. Int. Ed.* **2006,** *45* (23), 3748-3759.
4. Fürstner, A., Metathesis in total synthesis. *Chem. Commun.* **2011,** *47* (23), 6505.
5. Hoveyda, A. H.; Zhugralin, A. R., The remarkable metal-catalysed olefin metathesis reaction. *Nature* **2007,** *450* (7167), 243-251.
6. Banks, R. L.; Bailey, G. C., Olefin Disproportionation. A New Catalytic Process. *Ind. Eng. Chem. Prod. Res. Dev.* **1964,** *3* (3), 170-173.
7. Ivin, K. J.; Mol, J. C., Olefin metathesis and metathesis polymerization. Academic Press San Diego: San Diego, 1997.
8. Lwin, S.; Wachs, I. E., Olefin Metathesis by Supported Metal Oxide Catalysts. *ACS Catal.* **2014,** *4* (8), 2505-2520.
9. Mol, J. C., Industrial applications of olefin metathesis. *J. Mol. Catal.* **2004,** *213* (1), 39-45.
10. Mol, J. C.; van Leeuwen, P. W. N. M., Metathesis of Alkenes. In *Handbook of Heterogeneous Catalysis*, pp 3240-3256.
11. Grela, K., *Olefin metathesis : theory and practice*. Wiley Hoboken, New Jersey: Hoboken, New Jersey, 2014.
12. Higman, C. S.; Lummiss, J. A. M.; Fogg, D. E., Olefin Metathesis at the Dawn of Implementation in Pharmaceutical and Specialty-Chemicals Manufacturing. *Angew. Chem. Int. Ed.* **2016,** *55* (11), 3552-3565.
13. Hoveyda, A. H.; Malcolmson, S. J.; Meek, S. J.; Zhugralin, A. R., Catalytic Enantioselective Olefin Metathesis in Natural Product Synthesis. Chiral Metal-Based Complexes that Deliver High Enantioselectivity and More. *Angew. Chem. Int. Ed.* **2010,** *49* (1), 34-44.
14. Malcolmson, S. J.; Meek, S. J.; Sattely, E. S.; Schrock, R. R.; Hoveyda, A. H., Highly efficient molybdenum-based catalysts for enantioselective alkene metathesis. *Nature* **2008,** *456* (7224), 933-937.
15. Meek, S. J.; O'Brien, R. V.; Llaveria, J.; Schrock, R. R.; Hoveyda, A. H., Catalytic Z-selective olefin cross-metathesis for natural product synthesis. *Nature* **2011,** *471* (7339), 461-466.
16. Schrock, R. R.; Hoveyda, A. H., Molybdenum and tungsten imido alkylidene complexes as efficient olefin-metathesis catalysts. *Angew. Chem. Int. Ed.* **2003,** *42* (38), 4592-4633.
17. Leduc, A.-M.; Salameh, A.; Soulivong, D.; Chabanas, M.; Basset, J.-M.; Copéret, C.; Solans-Monfort, X.; Clot, E.; Eisenstein, O.; Böhm, V. P. W.; Röper, M., β-H Transfer from the Metallacyclobutane: A Key Step in the Deactivation and Byproduct Formation for the Well-Defined Silica-Supported Rhenium Alkylidene Alkene Metathesis Catalyst. *J. Am. Chem. Soc.* **2008,** *130* (19), 6288-6297.
18. Poater, A.; Solans-Monfort, X.; Clot, E.; Copéret, C.; Eisenstein, O., Understanding d^0-Olefin Metathesis Catalysts: Which Metal, Which Ligands? *J. Am. Chem. Soc.* **2007,** *129* (26), 8207-8216.
19. Solans-Monfort, X.; Clot, E.; Copéret, C.; Eisenstein, O., d^0 Re-Based Olefin Metathesis Catalysts, Re(≡CR)(=CHR)(X)(Y): The Key Role of X and Y Ligands for Efficient Active Sites. *J. Am. Chem. Soc.* **2005,** *127* (40), 14015-14025.
20. Solans-Monfort, X.; Coperet, C.; Eisenstein, O., Shutting Down Secondary Reaction Pathways: The Essential Role of the Pyrrolyl Ligand in Improving Silica Supported d0-ML4 Alkene Metathesis Catalysts from DFT Calculations. *J. Am. Chem. Soc.* **2010,** *132* (22), 7750-7757.
21. Solans-Monfort, X.; Copéret, C.; Eisenstein, O., Oxo vs Imido Alkylidene d^0-Metal Species: How and Why Do They Differ in Structure, Activity, and Efficiency in Alkene Metathesis? *Organometallics* **2012,** *31* (19), 6812-6822.
22. Solans-Monfort, X.; Copéret, C.; Eisenstein, O., Metallacyclobutanes from Schrock-Type d^0 Metal Alkylidene Catalysts: Structural Preferences and Consequences in Alkene Metathesis. *Organometallics* **2015,** *34* (9), 1668-1680.
23. Gordon, C. P.; Yamamoto, K.; Liao, W.-C.; Allouche, F.; Andersen, R. A.; Copéret, C.; Raynaud, C.; Eisenstein, O., Metathesis Activity Encoded in the Metallacyclobutane Carbon-13 NMR Chemical Shift Tensors. *ACS Cent. Sci.* **2017,** *3* (7), 759-768.
24. Gordon, C. P.; Shirase, S.; Yamamoto, K.; Andersen, R. A.; Eisenstein, O.; Copéret, C., NMR chemical shift analysis decodes olefin oligo- and polymerization activity of d^0 group 4 metal complexes. *Proc. Natl. Acad. Sci. U.S.A.* **2018,** *115* (26), E5867-E5876.
25. Yamamoto, K.; Gordon, C. P.; Liao, W.-C.; Copéret, C.; Raynaud, C.; Eisenstein, O., Orbital Analysis of Carbon-13 Chemical Shift Tensors Reveals Patterns to Distinguish Fischer and Schrock Carbenes. *Angew. Chem. Int. Ed.* **2017,** *56* (34), 10127-10131.
26. Halbert, S.; Copéret, C.; Raynaud, C.; Eisenstein, O., Elucidating the Link between NMR Chemical Shifts and Electronic Structure in d0 Olefin Metathesis Catalysts. *J. Am. Chem. Soc.* **2016,** *138* (7), 2261-2272.
27. Gordon, C. P.; Raynaud, C.; Andersen, R. A.; Copéret, C.; Eisenstein, O., Carbon-13 NMR Chemical Shift: A Descriptor for Electronic Structure and Reactivity of Organometallic Compounds. *Acc. Chem. Res.* **2019,** *52* (8), 2278-2289.
28. Gordon, C. P.; Copéret, C., Probing the Electronic Structure of Spectator Oxo Ligands by ^{17}O NMR Spectroscopy. *Chimia* **2020,** *74* (4), 225.
29. Bouhoute, Y.; Grekov, D.; Merle, N.; Szeto, K. C.; Larabi, C.; Del Rosal, I.; Maron, L.; Delevoye, L.; Gauvin, R. M.; Taoufik, M., On the use of ^{17}O NMR for understanding molecular and silica-grafted tungsten oxo siloxide complexes. *Dalton Trans.* **2023,** *52* (28), 9573-9581.
30. Berkson, Z. J.; Lätsch, L.; Hillenbrand, J.; Fü, A.; Copéret, C., Classifying and Understanding the Reactivities of Mo-Based Alkyne Metathesis Catalysts from ^{95}Mo NMR Chemical Shift Descriptors. *J. Am. Chem. Soc.* **2022,** *2022*, 15020-15025.
31. Berkson, Z. J.; Zhu, R.; Ehinger, C.; Lätsch, L.; Schmid, S. P.; Nater, D.; Pollitt, S.; Safonova, O. V.; Björgvinsdóttir, S.; Barnes, A. B.; Román-Leshkov, Y.; Price, G. A.; Sunley, G. J.; Copéret, C., Active Site Descriptors from ^{95}Mo NMR Signatures of Silica-Supported Mo-Based Olefin Metathesis Catalysts. *J. Am. Chem. Soc.* **2023,** *145* (23), 12651-12662.
32. Yakimov, A. V.; Kaul, C. J.; Kakiuchi, Y.; Sabisch, S.; Bolner, F. M.; Raynaud, J.; Monteil, V.; Berruyer, P.; Copéret, C., Well-Defined Ti Surface Sites in Ziegler–Natta Pre-Catalysts from $^{47/49}$Ti Solid-State Nuclear Magnetic Resonance Spectroscopy. *J. Phys. Chem. Lett.* **2024,** *15* (11), 3178-3184.

33. Lätsch, L.; Kaul, C. J.; Yakimov, A. V.; Müller, I. B.; Hassan, A.; Perrone, B.; Aghazada, S.; Berkson, Z. J.; De Baerdemaeker, T.; Parvulescu, A.-N.; Seidel, K.; Teles, J. H.; Copéret, C., NMR Signatures and Electronic Structure of Ti Sites in Titanosilicalite-1 from Solid-State $^{47/49}$Ti NMR Spectroscopy. *J. Am. Chem. Soc.* **2023,** *145* (28), 15018-15023.
34. Todisco, S.; Saielli, G.; Gallo, V.; Latronico, M.; Rizzuti, A.; Mastrorilli, P., 31P and 195Pt solid-state NMR and DFT studies on platinum(i) and platinum(ii) complexes. *Dalton Trans.* **2018,** *47* (27), 8884-8891.
35. Venkatesh, A.; Gioffrè, D.; Atterberry, B. A.; Rochlitz, L.; Carnahan, S. L.; Wang, Z.; Menzildjian, G.; Lesage, A.; Copéret, C.; Rossini, A. J., Molecular and Electronic Structure of Isolated Platinum Sites Enabled by the Expedient Measurement of 195Pt Chemical Shift Anisotropy. *J. Am. Chem. Soc.* **2022,** *144* (30), 13511-13525.
36. Venkatesh, A.; Lund, A.; Rochlitz, L.; Jabbour, R.; Gordon, C. P.; Menzildjian, G.; Viger-Gravel, J.; Berruyer, P.; Gajan, D.; Copéret, C.; Lesage, A.; Rossini, A. J., The Structure of Molecular and Surface Platinum Sites Determined by DNP-SENS and Fast MAS ^{195}Pt Solid-State NMR Spectroscopy. *J. Am. Chem. Soc*. **2020,** *142* (44), 18936-18945.
37. Wang, Z.; Völker, L. A.; Robinson, T. C.; Kaeffer, N.; Menzildjian, G.; Jabbour, R.; Venkatesh, A.; Gajan, D.; Rossini, A. J.; Copéret, C.; Lesage, A., Speciation and Structures in Pt Surface Sites Stabilized by N-Heterocyclic Carbene Ligands Revealed by Dynamic Nuclear Polarization Enhanced Indirectly Detected ^{195}Pt NMR Spectroscopic Signatures and Fingerprint Analysis. *J. Am. Chem. Soc.* **2022,** *144* (47), 21530-21543.
38. Sabisch, S.; Kakiuchi, Y.; Docherty, S. R.; Yakimov, A. V.; Copéret, C., Geometry and Local Environment of Surface Sites in Vanadium-Based Ziegler–Natta Catalysts from ^{51}V Solid-State NMR Spectroscopy. *J. Am. Chem. Soc.* **2023,** *145* (47), 25595-25603.
39. Kress, J.; Osborn, J. A., Tungsten carbene complexes in olefin metathesis: a cationic and chiral active species. *J. Am. Chem. Soc.* **1983,** *105* (20), 6346-6347.
40. Kress, J.; Osborn, J. A., Detection of the Tungsten–Carbene–Olefin Intermediates in Catalytic Metathesis Systems Containing High-Valent Metal Centers. *Angew. Chem. Int. Ed.* **1992,** *31* (12), 1585-1587.
41. Kress, J.; Wesolek, M.; Osborn, J. A., Tungsten (IV) carbenes for the metathesis of olefins. Direct observation and identification of the chain carrying carbene complexes in a highly active catalyst system. *J. Chem. Soc., Chem. Commun.* **1982,** (9), 514-516.
42. Herz, K.; Podewitz, M.; Stöhr, L.; Wang, D.; Frey, W.; Liedl, K. R.; Sen, S.; Buchmeiser, M. R., Mechanism of Olefin Metathesis with Neutral and Cationic Molybdenum Imido Alkylidene N-Heterocyclic Carbene Complexes. *J. Am. Chem. Soc.* **2019,** *141* (20), 8264-8276.
43. Schowner, R.; Frey, W.; Buchmeiser, M. R., Cationic Tungsten-Oxo-Alkylidene-N-Heterocyclic Carbene Complexes: Highly Active Olefin Metathesis Catalysts. *J. Am. Chem. Soc.* **2015,** *137* (19), 6188-6191.
44. Pucino, M.; Mougel, V.; Schowner, R.; Fedorov, A.; Buchmeiser, M. R.; Copéret, C., Cationic Silica-Supported N-Heterocyclic Carbene Tungsten Oxo Alkylidene Sites: Highly Active and Stable Catalysts for Olefin Metathesis. *Angew. Chem. Int. Ed.* **2016,** *55* (13), 4300-4302.
45. Benedikter, M. J.; Musso, J. V.; Frey, W.; Schowner, R.; Buchmeiser, M. R., Cationic Group VI Metal Imido Alkylidene *N* - Heterocyclic Carbene Nitrile Complexes: Bench - Stable, Functional - Group - Tolerant Olefin Metathesis Catalysts. *Angew. Chem. Int. Ed.* **2021,** *60* (3), 1374-1382.
46. Buchmeiser, M. R., Molybdenum Imido, Tungsten Imido and Tungsten Oxo Alkylidene N-Heterocyclic Carbene Olefin Metathesis Catalysts. *Chem. Eur. J.* **2018,** *24* (54), 14295-14301.
47. Buchmeiser, M. R.; Sen, S.; Unold, J.; Frey, W., N-heterocyclic carbene, high oxidation state molybdenum alkylidene complexes: Functional-group-tolerant cationic metathesis catalysts. *Angew. Chem. Int. Ed.* **2014,** *53* (35), 9384-9388.
48. Hauser, P. M.; Van Der Ende, M.; Groos, J.; Frey, W.; Wang, D.; Buchmeiser, M. R., Tungsten Alkylidynes Cationic Tungsten Alkylidyne N-Heterocyclic Carbene Complexes: Synthesis and Reactivity in Alkyne Metathesis. **2020**.
49. Imbrich, D. A.; Elser, I.; Frey, W.; Buchmeiser, M. R., First Neutral and Cationic Tungsten Imido Alkylidene N-Heterocyclic Carbene Complexes. *ChemCatChem* **2017,** *9* (15), 2996-3002.
50. Musso, J. V.; De Jesus Silva, J.; Benedikter, M. J.; Groos, J.; Frey, W.; Copéret, C.; Buchmeiser, M. R., Cationic molybdenum oxo alkylidenes stabilized by N-heterocyclic carbenes: from molecular systems to efficient supported metathesis catalysts. *Chem. Sci.* **2022,** *13* (29), 8649-8656.
51. Sen, S.; Schowner, R.; Imbrich, D. A.; Frey, W.; Hunger, M.; Buchmeiser, M. R., Neutral and Cationic Molybdenum Imido Alkylidene N-Heterocyclic Carbene Complexes: Reactivity in Selected Olefin Metathesis Reactions and Immobilization on Silica. *Chem. Eur. J.* **2015,** *21* (39), 13778-13787.
52. Carmona, E.; Sánchez, L.; Poveda, M. L.; Jones, R. A.; Hefner, J. G., Some trimethyl phosphine and trimethyl phosphite complexes of tungsten(IV). *Polyhedron* **1983,** *2* (8), 797-801.
53. Sharp, P. R.; Bryan, J. C.; Mayer, J. M.; Templeton, J. L.; Feng, S., Tungsten Chloro Phosphine Complexes. In *Inorganic Syntheses*, 1990; pp 326-332.
54. Luz, C.; Glok, E.; Horrer, G.; Radius, U., N-heterocyclic carbene and cyclic (alkyl)(amino)carbene complexes of molybdenum(IV) and tungsten(IV). *Dalton Trans.* **2022,** *51* (47), 18337-18352.
55. Agapie, T.; Diaconescu, P. L.; Cummins, C. C., Methine (CH) Transfer via a Chlorine Atom Abstraction/Benzene-Elimination Strategy: Molybdenum Methylidyne Synthesis and Elaboration to a Phosphaisocyanide Complex. *J. Am. Chem. Soc.* **2002,** *124* (11), 2412-2413.
56. Peters, J. C.; Odom, A. L.; Cummins, C. C., A terminal molybdenum carbide prepared by methylidyne deprotonation. *Chem. Commun.* **1997,** (20), 1995-1996.
57. Churchill, M. R.; Rheingold, A. L.; Wasserman, H. J., Structural Studies on Tungsten-Methylidyne Complexes. Molecular Geometry of W(≡CH)(Cl)$(PMe_3)_4$ and W(≡CH•$AlMe_{2-x}Cl_{1+x}$)(Cl)$(PMe_3)_3$ ($x \approx 0.18$), a Lewis Acid Adduct of the Tungsten-Methylidyne Triple Bond. *Inorg. Chem.* **1981,** *20* (10), 3392-3399.
58. Enriquez, A. E.; White, P. S.; Templeton, J. L., Reactions of an amphoteric terminal tungsten methylidyne complex. *J. Am. Chem. Soc.* **2001,** *123* (21), 4992-5002.
59. Hill, A. F.; Ward, J. S.; Xiong, Y., Synthesis of a Stable Methylidyne Complex. *Organometallics* **2015,** *34* (20), 5057-5064.
60. Holmes, S. J.; Schrock, R. R.; Rowen Churchill, M.; Wasserman, H. J., Some Reactions of Tungsten Methylidyne Complexes and the Crystal Structure of $[W_2(CPMe_3)_2(PMe_3)_4Cl_4][AlCl_4]_2$. *Organometallics* **1984,** *3* (3), 476-484.
61. Sharp, P. R.; Holmes, S. J.; Schrock, R. R.; Churchill, M. R.; Wasserman, H. J., Tungsten Methylidyne Complexes. *J. Am. Chem. Soc.* **1981,** *103* (4), 965-966.
62. van der Eide, E. F.; Piers, W. E.; Parvez, M.; McDonald, R., Synthesis and Characterization of Cationic Tungsten(V) Methylidynes. *Inorg. Chem.* **2007,** *46* (1), 14-21.
63. Buss, J. A.; Bailey, G. A.; Oppenheim, J.; VanderVelde, D. G.; Goddard, W. A., III; Agapie, T., CO Coupling Chemistry of a Terminal Mo Carbide: Sequential Addition of Proton, Hydride, and CO Releases Ethenone. *J. Am. Chem. Soc.* **2019,** *141* (39), 15664-15674.
64. Joost, M.; Transue, W. J.; Cummins, C. C., Diazomethane umpolung atop anthracene: an electrophilic methylene transfer reagent. *Chem. Sci.* **2018,** *9* (6), 1540-1543.
65. Kurogi, T.; Carroll, P. J.; Mindiola, D. J., A Terminally Bound Niobium Methylidyne. *J. Am. Chem. Soc.* **2016,** *138* (13), 4306-4309.
66. Kurogi, T.; Mindiola, D. J., Methylidyne Transfer as a Plausible Deactivation Pathway for Ynene Metathesis. *Organometallics* **2020,** *39* (24), 4474-4478.
67. Kurogi, T.; Pinter, B.; Mindiola, D. J., Methylidyne Transfer Reactions with Niobium. *Organometallics* **2018,** *37* (20), 3385-3388.
68. Holmes, S. J.; Schrock, R. R., A tungsten T-shaped methylene complex and related methylidyne hydride complexes. *J. Am. Chem. Soc.* **1981,** *103* (15), 4599-4600.

69. Schrock, R. R.; Seidel, S. W.; Mösch-Zanetti, N. C.; Shih, K.-Y.; O'Donoghue, M. B.; Davis, W. M.; Reiff, W. M., Synthesis and Decomposition of Alkyl Complexes of Molybdenum(IV) That Contain a $[(Me_3SiNCH_2CH_2)_3N]^{3-}$ Ligand. Direct Detection of α-Elimination Processes That Are More than Six Orders of Magnitude Faster than β-Elimination Processes. *J. Am. Chem. Soc.* **1997,** *119* (49), 11876-11893.
70. Shih, K.-Y.; Totland, K.; Seidel, S. W.; Schrock, R. R., Spontaneous Loss of Molecular Hydrogen from Tungsten(IV) Alkyl Complexes To Give Alkylidyne Complexes. *J. Am. Chem. Soc.* **1994,** *116* (26), 12103-12104.
71. Listemann, M. L.; Schrock, R. R., Multiple metal carbon bonds. 35. A general route to tri-tert-butoxytungsten alkylidyne complexes. Scission of acetylenes by ditungsten hexa-tert-butoxide. *Organometallics* **1985,** *4* (1), 74-83.
72. Abernethy, C. D.; Codd, G. M.; Spicer, M. D.; Taylor, M. K., A highly stable N-heterocyclic carbene complex of trichloro-oxo-vanadium(V) displaying novel Cl-Ccarbene bonding interactions. *J. Am. Chem. Soc.* **2003,** *125* (5), 1128-1129.
73. Bryan, J. C.; Geib, S. J.; Rheingold, A. L.; Mayer, J. M., Oxidative addition of carbon dioxide, epoxides, and related molecules to $WCl_2(PMePh_2)_4$ yielding tungsten(IV) oxo, imido, and sulfido complexes. Crystal and molecular structure of $W(O)Cl_2(CO)(PMePh_2)_2$. *J. Am. Chem. Soc.* **1987,** *109* (9), 2826-2828.
74. Bryan, J. C.; Mayer, J. M., Oxidative addition of cyclopentanone to $WCl_2(PMePh_2)_4$ to give a tungsten(VI) oxo-alkylidene complex. *J. Am. Chem. Soc.* **1987,** *109* (23), 7213-7214.
75. Bryan, J. C.; Mayer, J. M., Oxidative addition of carbon-oxygen and carbon-nitrogen double bonds to $WCl_2(PMePh_2)_4$. Synthesis of tungsten metallaoxirane and tungsten oxo- and imido-alkylidene complexes. *J. Am. Chem. Soc.* **1990,** *112* (6), 2298-2308.
76. Hillenbrand, J.; Leutzsch, M.; Gordon, C. P.; Copéret, C.; Fürstner, A., 183 W NMR Spectroscopy Guides the Search for Tungsten Alkylidyne Catalysts for Alkyne Metathesis. *Angew. Chem. Int. Ed.* **2020,** *59* (48), 21758-21768.
77. Eberle, L.; Ballmann, J., Synthesis of Collidine from Dinitrogen via a Tungsten Nitride. *J. Am. Chem. Soc.* **2024,** *146* (12), 7979-7984.
78. Carbajo, R. J.; Zhang, L.; López-Ortiz, F., ^{183}W NMR study of alkenylcarbyne– and alkenylvinylidene–tungsten complexes. *Magn. Reson. Chem.* **1998,** *36* (11), 807-814.
79. Kakiuchi, Y.; Karmakar, P. S.; Roudin, J.; Tonks, I. A.; Copéret, C., Bonding and Reactivity of d^0 Transition Metal Imido Complexes Encoded in Their ^{15}N NMR Signatures. *J. Am. Chem. Soc.* **2024**, *146*, 9860–9870.
80. Widdifield, C. M.; Schurko, R. W., Understanding chemical shielding tensors using group theory, MO analysis, and modern density-functional theory. *Concepts Magn. Reson., Part A* **2009,** *34A* (2), 91-123.
81. Ramsey, N. F., Magnetic Shielding of Nuclei in Molecules. *Phys. Rev.* **1950,** *78* (6), 699-703.
82. Autschbach, J., Analyzing NMR shielding tensors calculated with two-component relativistic methods using spin-free localized molecular orbitals. *Chem. Phys.* **2008,** *128* (16).
83. Bohmann, J. A.; Weinhold, F.; Farrar, T. C., Natural chemical shielding analysis of nuclear magnetic resonance shielding tensors from gauge-including atomic orbital calculations. *Chem. Phys.* **1997,** *107* (4), 1173-1184.
84. Greco, J. B.; Peters, J. C.; Baker, T. A.; Davis, W. M.; Cummins, C. C.; Wu, G., Atomic Carbon as a Terminal Ligand: Studies of a Carbidomolybdenum Anion Featuring Solid-State ^{13}C NMR Data and Proton-Transfer Self-Exchange Kinetics. *J. Am. Chem. Soc.* **2001,** *123* (21), 5003-5013.
85. Berkson, Z. J.; Bernhardt, M.; Copéret, C., Solid-State ^{183}W NMR Spectroscopy as a High-Resolution Probe of Polyoxotungstate Structures and Dynamics. *J. Phys. Chem. Lett.* **2024,** *15* (7), 1950-1955.
86. For detailed comparison of experimental value versus cal-culation, see the ESI file.
87. Bagno, A.; Bonchio, M.; Sartorel, A.; Scorrano, G., Relativistic DFT Calculations of Polyoxotungstate ^{183}W NMR Spectra: Insight into their Solution Structure. *ChemPhysChem* **2003,** *4* (5), 517-519.
88. Kazansky, L. P.; Yamase, T., Electronic Population on Tungsten, Molybdenum, and Vanadium Atoms and ^{183}W, ^{95}Mo, and ^{51}V NMR in Polyoxometalates. *J. Phys. Chem. A* **2004,** *108* (30), 6437-6448.
89. Gessner, V. H.; Meier, F.; Uhrich, D.; Kaupp, M., Synthesis and Bonding in Carbene Complexes of an Unsymmetrical Dilithio Methandiide: A Combined Experimental and Theoretical Study. *Chem. Eur. J.* **2013,** *19* (49), 16729-16739.
90. Estes, D. P.; Gordon, C. P.; Fedorov, A.; Liao, W. C.; Ehrhorn, H.; Bittner, C.; Zier, M. L.; Bockfeld, D.; Chan, K. W.; Eisenstein, O.; Raynaud, C.; Tamm, M.; Copéret, C., Molecular and Silica-Supported Molybdenum Alkyne Metathesis Catalysts: Influence of Electronics and Dynamics on Activity Revealed by Kinetics, Solid-State NMR, and Chemical Shift Analysis. *J. Am. Chem. Soc.* **2017,** *139* (48), 17597-17607.
91. Gordon, C. P.; Culver, D. B.; Conley, M. P.; Eisenstein, O.; Andersen, R. A.; Copéret, C., π-Bond Character in Metal–Alkyl Compounds for C–H Activation: How, When, and Why? *J. Am. Chem. Soc.* **2019,** *141* (1), 648-656.
92. Kaupp, M., Interpretation of NMR Chemical Shifts. In *Calculation of NMR and EPR Parameters*, 2004; pp 293-306.
93. Anhaus, J. T.; Kee, T. P.; Schofield, M. H.; Schrock, R. R., Planar "20-electron" osmium imido complexes. A linear imido ligand does not necessarily donate its lone pair of electrons to the metal. *J. Am. Chem. Soc.* **1990,** *112* (4), 1642-1643.
94. Benson, M. T.; Bryan, J. C.; Burrell, A. K.; Cundari, T. R., Bonding and Structure of Heavily π-Loaded Complexes. *Inorg. Chem.* **1995,** *34* (9), 2348-2355.
95. Chao, Y. W.; Rodgers, P. M.; Wigley, D. E.; Alexander, S. J.; Rheingold, A. L., Tris(phenylimido) complexes of tungsten: preparation and properties of the d^0 $W(=NR)_3$ functional group. *J. Am. Chem. Soc.* **1991,** *113* (16), 6326-6328.
96. O'Reilly, M. E.; Ghiviriga, I.; Abboud, K. A.; Veige, A. S., A New ONO^{3-} Trianionic Pincer-Type Ligand for Generating Highly Nucleophilic Metal–Carbon Multiple Bonds. *J. Am. Chem. Soc.* **2012,** *134* (27), 11185-11195.
97. Gonsales, S. A.; Pascualini, M. E.; Ghiviriga, I.; Abboud, K. A.; Veige, A. S., Fast "Wittig-Like" Reactions As a Consequence of the Inorganic Enamine Effect. *J. Am. Chem. Soc.* **2015,** *137* (14), 4840-4845.
98. Ehinger, C.; Gordon, C. P.; Copéret, C., Oxygen transfer in electrophilic epoxidation probed by ^{17}O NMR: differentiating between oxidants and role of spectator metal oxo. *Chem. Sci.* **2019,** *10* (6), 1786-1795.
99. Rappé, A. K.; Goddard, W. A., Bivalent spectator oxo bonds in metathesis and epoxidation alkenes. *Nature* **1980,** *285* (5763), 311-312.
100. Rappe, A. K.; Goddard, W. A., Mechanism of metathesis and epoxidation in chromium and molybdenum complexes containing methyl-oxo bonds. *J. Am. Chem. Soc.* **1980,** *102* (15), 5114-5115.
101. Rappe, A. K.; Goddard, W. A., Olefin metathesis - a mechanistic study of high-valent Group VI catalysts. *J. Am. Chem. Soc.* **1982,** *104* (2), 448-456.
102. Copéret, C.; Berkson, Z. J.; Chan, K. W.; De Jesus Silva, J.; Gordon, C. P.; Pucino, M.; Zhizhko, P. A., Olefin metathesis: what have we learned about homogeneous and heterogeneous catalysts from surface organometallic chemistry? *Chem. Sci.* **2021,** *12* (9), 3092-3115.
103. Poater, A.; Solans-Monfort, X.; Clot, E.; Copéret, C.; Eisenstein, O., DFT calculations of d^0 M(NR)(CH*t*Bu)(X)(Y) (M = Mo, W; R = CPh_3, 2,6-*i*Pr–C_6H_3; X and Y = CH_2*t*Bu, O*t*Bu, OSi(O*t*Bu)$_3$) olefin metathesis catalysts: structural, spectroscopic and electronic properties. *Dalton Trans.* **2006,** (25), 3077-3087.
104. Kaltsoyannis, N.; Mountford, P., Theoretical study of the geometric and electronic structures of pseudo-octahedral d^0 imido compounds of titanium: the trans influence in mer-$[Ti(NR)Cl_2(NH_3)_3]$ (R = Bu^t, C_6H_5 or $C_6H_4NO_2$-4). *J. Chem. Soc., Dalton Trans.* **1999,** (5), 781-790.
105. Parsons, T. B.; Hazari, N.; Cowley, A. R.; Green, J. C.; Mountford, P., Synthesis, Structures, and DFT Bonding Analysis of New Titanium Hydrazido(2−) Complexes. *Inorg. Chem.* **2005,** *44* (23), 8442-8458.
106. Chabanas, M.; Baudouin, A.; Copéret, C.; Basset, J.-M., A Highly Active Well-Defined Rhenium Heterogeneous Catalyst for Olefin Metathesis Prepared via Surface Organometallic Chemistry. *J. Am. Chem. Soc.* **2001,** *123* (9), 2062-2063.

107. Gordon, C. P.; Lätsch, L.; Copéret, C., Nuclear Magnetic Resonance: A Spectroscopic Probe to Understand the Electronic Structure and Reactivity of Molecules and Materials. *J. Phys. Chem. Lett.* **2021,** *12* (8), 2072-2085.

.